AMERICAN METEOROLOGICAL SOCIETY

*Bulletin of the American Meteorological Society*



The DOI for this manuscript is doi: 10.1175/BAMS-D-15-00142.1

# The Saharan Aerosol Long-range TRansport and Aerosol-Cloud-Interaction Experiment (SALTRACE): overview and selected highlights

Bernadett Weinzierl[1,2], A. Ansmann[3], J. M. Prospero[4], D. Althausen[3], N. Benker[7], F. Chouza[1], M. Dollner[2,5], D. Farrell[6], W. K. Fomba[3], V. Freudenthaler[5], J. Gasteiger[2,5], S. Groß[1], M. Haarig[3], B. Heinold[3], K. Kandler[7], T. B. Kristensen[3], O. L. Mayol-Bracero[8], T. Müller[3], O. Reitebuch[1], D. Sauer[1], A. Schäfler[1], K. Schepanski[3], A. Spanu[2,1], I. Tegen[3], C. Toledano[9], A. Walser[5,1]

[1] Deutsches Zentrum für Luft- und Raumfahrt (DLR), Oberpfaffenhofen, Germany

[2] University of Vienna (UNIVIE), Aerosol Physics and Environmental Physics, Wien, Austria

[3] Leibniz Institute for Tropospheric Research (TROPOS), Leipzig, Germany

[4] University of Miami, Miami, USA

[5] Ludwig-Maximilians-Universität (LMU), Meteorologisches Institut, München, Germany

[6] Caribbean Institute for Meteorology and Hydrology (CIMH), Bridgetown, Barbados

[7] Technische Universität Darmstadt, Institut für Angewandte Geowissenschaften, Darmstadt, Germany

[8] University of Puerto Rico, Department of Environmental Science, San Juan, USA

[9] Universidad de Valladolid, Grupo de Óptica Atmosférica, Valladolid, Spain

**Corresponding Author:** Bernadett Weinzierl (bernadett.weinzierl@univie.ac.at)

**Corresponding author address:** University of Vienna, Aerosol Physics and Environmental Physics, Boltzmanngasse 5, A-1090 Wien, AUSTRIA

**Abstract (max. 260 words) – 260 words**

North Africa is the world's largest source of dust, a large part of which is transported across the Atlantic to the Caribbean and beyond where it can impact radiation and clouds. Many aspects of this transport and its climate effects remain speculative. The Saharan Aerosol Long-range Transport and Aerosol-Cloud-Interaction Experiment (SALTRACE: http://www.pa.op.dlr.de/saltrace) linked ground-based and airborne measurements with remote-sensing and modeling techniques to address these issues in a program that took place in 2013-2014. Specific objectives were: to (1) characterize the chemical, microphysical and optical properties of dust in the Caribbean, (2) quantify the impact of physical and chemical changes ("aging") on the radiation budget and cloud-microphysical processes, (3) investigate the meteorological context of trans-Atlantic dust transport, and (4) assess the roles of removal processes during transport.

SALTRACE was a German-led initiative involving scientists from Europe, Cabo Verde, the Caribbean and the US. The Falcon research aircraft of the Deutsches Zentrum für Luft- und Raumfahrt (DLR), equipped with a comprehensive aerosol and wind-lidar payload, played a central role. Several major dust outbreaks were studied with 86 hours of flight time under different conditions making it by far the most extensive investigation on long-range transported dust ever made.

This article presents an overview of SALTRACE and highlights selected results including data from trans-Atlantic flights in coherent air masses separated by more than 4,000 km distance that enabled measurements of transport effects on dust properties.

SALTRACE will improve our knowledge on the role of mineral dust in the climate system and provide data for studies on dust-interactions with clouds, radiation and health.

46 **Capsule Summary**

47 The aircraft and ground-based SALTRACE campaign in the tropical Atlantic in 2013 – 2014
48 characterizes the large-scale transport of African dust, dust "aging" during transit, and its
49 impact on radiation and cloud-microphysics.

50

51

52

53

54

55

56

57

58

59

60

61

62

63

## 1. Introduction

Although substantial effort has been undertaken in the last decades to improve our knowledge about the role of aerosols in the climate system, aerosols and clouds still pose the largest uncertainty to estimates and interpretations of the Earth's changing energy budget (IPCC, 2013). Among aerosols, mineral dust particles (hereafter, simply "dust particles" or "dust") are of key importance because they contribute to about half of the global annual particle emissions by mass (Hinds, 1999; Huneeus et al., 2011), significantly impact the radiation budget of the Earth by scattering, absorption and emission of solar and terrestrial radiation (Sokolik et al., 2001; Tegen, 2003; Balkanski et al., 2007), act as cloud condensation nuclei (CCN), and have been identified as effective ice nucleating particles (INP; Hoose and Möhler, 2012). Deposited dust can be a significant nutrient to the ocean (Jickells et al., 2005; Maher et al., 2010; Niedermeier et al., 2014). In addition, dust may have a severe impact on aviation by causing poor visibility (Weinzierl et al., 2012) affecting the take-off and landing of aircraft. Last but not least, there is increasing evidence that dust might be a human health concern (Goudie, 2014; Morman and Plumlee, 2014).

The major dust source regions are located in the Northern Hemisphere and extend from the west coast of North Africa, through the Middle East, to Central Asia and China. AeroCom models estimate that North Africa including the Sahara emits about 200 to 3000 Tg of dust every year, thereby contributing about 70% to the total global dust emission (Huneeus et al., 2011). African dust is regularly transported westwards across the Atlantic Ocean to the Caribbean (e.g. Prospero, 1999; Prospero and Lamb, 2003; Stevens et al., 2015), the southern United States (Prospero, 1999), and northeastern South America (Swap et al., 1992; Prospero et al., 2014).

During the summer months the main dust transport takes place in the Saharan Air Layer (SAL), a hot, dry, elevated layer that has its origins over the Sahara desert (Carlson and Prospero, 1972; Prospero and Carlson, 1972). The SAL often covers large parts of the tropical Atlantic Ocean and can be easily tracked by satellite observations of aerosol optical depth (AOD) and lidar (e.g. Liu et al., 2008; Chouza et al., 2016a). Presently, the SAL is attracting great interest because it is suspected to influence tropical cyclone activity (e.g. Dunion and Velden, 2004; Braun, 2010; Evan et al., 2011; Peng et al., 2012; Brammer and Thorncroft, 2015; Hankes et al., 2015). However, the details of this influence are not yet understood.

In the past decade several comprehensive airborne dust field experiments including the Saharan Mineral Dust Experiment (SAMUM-1, Heintzenberg, 2009; SAMUM-2, Ansmann et al., 2011) were performed in the vicinity of the Sahara and in the outflow region of African dust in the Cabo Verde area. Table 1 and references therein give an overview over major airborne dust field experiments over Africa, the Atlantic Ocean, and in the Caribbean. Although a few airborne dust campaigns focused on the Caribbean, most of these previous measurements in the Caribbean only covered altitudes below 3 km, and they lacked of the extensive instrumentation available to us in SALTRACE. Recent ground-based measurements at the Caribbean island of Puerto Rico studied African dust size distribution, optical properties, dust-cloud impacts (Spiegel et al., 2014; Raga et al., 2016), and chemical composition (Gioda et al., 2013; Denjean et al., 2015; Fitzgerald et al., 2015; Denjean et al., 2016; Valle-Diaz et al., 2016).

Despite substantial progress, many questions concerning the role of dust in the climate system remain open (e.g. Ansmann et al., 2011; Ryder et al., 2015). For example, the uncertainty of IPCC Assessment Report 5 estimates for global average direct radiative forcing by anthropogenic mineral dust aerosol which is assumed to be 20% of total dust is [-0.3; +0.1]

111 $Wm^{-2}$ (Table 8.4 in Myhre et al., 2013). This range has not changed since the previous IPCC
112 report in 2007, indicating further research needs.

113 A critical parameter for the derivation of radiative forcing estimates is the particle size
114 distribution which is set at emission (Mahowald et al., 2014), but changes during long-range
115 transport. For example, preferably large super-micron dust particles are lost through
116 gravitational settling and efficient particle aging occurs when particles act as CCN and INP
117 (Pöschl, 2005). Cloud-processing is one possible pathway producing sulfate-coated dust
118 particles and changing the aerosol size spectrum (e.g. Levin et al., 1996; Wurzler et al., 2000),
119 thus changing the probability of rain formation and influencing wet deposition of dust. Recent
120 laboratory measurements indicate that dust particles may become better CCN after cloud
121 processing (Kumar et al., 2011). Understanding the very complex interaction between
122 aerosols, clouds and precipitation is challenging and requires comprehensive, coordinated and
123 long-term measurements and state-of-the-art modeling (Stevens and Feingold, 2009). Many
124 models have attempted to simulate the effects of aging (e.g. Abdelkader et al., 2015), but it is
125 difficult to assess the validity of these results because of the absence of data with which to
126 test the effect.

127 In a recent review Mahowald et al. (2014) concluded that new measurements of dust size
128 distributions agree roughly within the size range between 0.1-5 µm particle diameter, but
129 below and above this size range, the dust size distribution is not well understood. In particular,
130 it is not clear, why in-situ observations generally lead to considerably larger mean particle
131 sizes than retrievals from remote sensing instruments (Reid et al., 2003a; Müller et al., 2010;
132 Toledano et al., 2011). This is particularly important for radiative forcing estimates, as the
133 coarse mode size distribution has a strong impact on the radiative budget and can even switch
134 the sign of the radiative forcing from a net cooling to heating (Otto et al., 2007).

These various studies demonstrate that dust is associated with a significant climate effect and may have a substantial impact on cloud processes and, furthermore, that particle aging might enhance these effects. We lack the understanding of the processes that lead to mixing of dust with other aerosols and of the factors that affect dust deposition.

In SALTRACE we collected a unique data set which provides new insights into these processes. This article presents an overview of the SALTRACE program and highlights important results. In Section 2, we introduce the SALTRACE measurement sites, intensive observation periods, and instrumentation. Section 3 evaluates the SALTRACE measurements in the context of the 50-year Barbados dust record. Section 4 and 5 describe the dust source activity during SALTRACE and follow with the conceptual "big picture" of trans-Atlantic dust transport. Section 6 highlights selected SALTRACE results and discusses the modification of dust during trans-Atlantic transport, the passage of tropical storm Chantal and its impact on the dust layer structure, and dust as a reservoir/source for CCN and INP.

## 2. Overview of the SALTRACE project

The Saharan Aerosol Long-range Transport and Aerosol-Cloud-Interaction Experiment (SALTRACE: http://www.pa.op.dlr.de/saltrace) was conducted from spring 2013 until summer 2014. Table 2 gives an overview of activities performed within the SALTRACE framework. The core of the SALTRACE program was an atmospheric column closure experiment[1] in June/July 2013 involving ground-based and airborne in-situ and remote sensing observations in Barbados (main super-site), Puerto Rico and Cabo Verde. For the airborne SALTRACE

[1] Atmospheric column closure experiments aim to characterize the same parameters of a system with different, independent methods and models to minimize the measurement uncertainties through comparison of the derived values.

155 measurements, the DLR research aircraft Falcon was equipped with a suite of in-situ
156 instruments for the determination of microphysical and optical aerosol properties, and with
157 sampling devices for offline particle analysis, a nadir-looking 2-µm wind lidar, dropsondes and
158 instruments for standard meteorological parameters. Details about the instrumentation at the
159 main super-site Barbados and on the research aircraft as well as accompanied modeling
160 activities at large-eddy and regional scale are given in Table 3 (supplemental material). Before
161 the measurements in June/July 2013, a cruise of the research vessel Meteor between
162 Guadeloupe and Cabo Verde took place in April/May 2013 (Kanitz et al., 2014). Later, in
163 February/March 2014 (SALTRACE-2) and June/July 2014 (SALTRACE-3), additional intensive
164 ground-based lidar and sun photometer observations followed to cover the annual variability
165 of dust flow into the Caribbean (Table 2).

166 Figure 1 sketches the airborne SALTRACE observations in summer 2013 including flight tracks
167 (red lines). Figure 2 shows the Falcon base at Grantley International Airport together with the
168 measurement locations of the in-situ and remote-sensing measurements on Barbados. In total
169 31 research flights were performed. The DLR research aircraft Falcon spent more than 86 flight
170 hours studying dust from several dust outbreaks under a variety of atmospheric conditions
171 between Senegal, Cabo Verde, the Caribbean, and Florida.

172 A detailed list of SALTRACE flights including take-off time, landing time and objective is
173 provided in the supplemental material (Table 4). The flights in the Cabo Verde region (11-17
174 June 2013) aimed to characterize dust close to the source region and are also used for
175 comparison with data from SAMUM-2 measurements (January/February 2008) in the Cabo
176 Verde area (Ansmann et al., 2011; Weinzierl et al., 2011, and the references therein). The first
177 part of the research flights in the Caribbean (20-26 June 2013) studied the horizontal
178 variability of dust properties with extended east-west and north-south sampling flights and

included the trans-Atlantic dust sampling of the same air mass on both sides of the Atlantic (17 and 22 June 2013). The flights on 30 June and 1 July were intended to investigate the variability of dust properties between Barbados, Antigua and Puerto Rico and to study the wet deposition of dust. The second half of the measurements (5-12 July 2013) focused on extended vertical profiling over the Atlantic east of Barbados, over the lidar and ground-sites on Barbados, and west of the Caribbean islands to study downwind transport from Barbados and island effects (Chouza et al., 2016b; Jähn et al., 2016). Furthermore, we had the unique opportunity to make measurements before, during and after the passage of tropical storm Chantal (8-10 July 2013). To our knowledge, these are the first measurements of dust conditions in the vicinity of such a storm ever made with an extensive aerosol instrument package. A second sequence of dust sampling flights was performed towards Puerto Rico and into the Bahamas/Florida area (11-13 July 2013). The flight program culminated with a route that took the Falcon along the east coast of the US, across the high-latitude North Atlantic and back to our home base in Germany. During the flights back to Germany, the Falcon encountered thick smoke layers where refractory black carbon mass mixing ratios reached values as high as 100-380 ng $kg^{-1}$, higher than the values around 270 ng $kg^{-1}$ observed in an intense smoke layer in the upper troposphere over Germany originating from the pyro-convective Pagami Creek fire (Minnesota, USA) (Dahlkötter et al., 2014).

## 3. SALTRACE in the context of the 50-year Barbados dust record

Barbados was chosen as main super-site for SALTRACE because it is the easternmost island of the Caribbean which enables measurements of undisturbed African dust layers after they transit the Atlantic. Furthermore Barbados has the world's longest record of ground-based

dust measurements which started in 1965 and continues today (Prospero and Lamb, 2003; Prospero et al., 2014) allowing us to evaluate the SALTRACE data in long-term context.

Dust transport follows a pronounced seasonal cycle with a minimum in winter and a maximum in summer peaking in June-July-August (Doherty et al., 2008; Prospero et al., 2014). Figure 3 depicts average summer (June-July-August) dust mass concentration values measured at Ragged Point, Barbados, between 1965 and 2013. The years of the SAMUM and SALTRACE measurements are indicated in red. Average summer dust mass concentrations vary between less than 10 and around 50 µg $m^{-3}$ from year to year. The periods of high dust concentrations in the early 1970s and in the mid-1980s were linked to drought conditions in Africa (Prospero and Lamb, 2003; Prospero et al., 2014), and the variability of the winds over the Sahara has been shown to impact in the dust load over the Atlantic (Wang et al., 2015; Evan et al., 2016). The causes of the variation in dust transport since the 1980s are still a subject of research and numerous efforts have been made to relate the Barbados dust record to various climate indices, e.g., El Niño Southern Oscillation (ENSO) (Prospero and Lamb, 2003; DeFlorio et al., 2016), North Atlantic Oscillation (NAO) (Ginoux et al., 2004; Evan et al., 2006), Atlantic Multidecadal Oscillation (AMO) (Evan et al., 2011; Wang et al., 2012; DeFlorio et al., 2016). Of these the AMO seems to have played a particularly strong role. However it is notable that high concentrations in 1997-1998 were coincident with an exceptionally strong El Niño. Since about 1970, excepting the periods of high concentration in summer, low summer mean values seem to fall between 15 to 20 µg $m^{-3}$ which might be thought of as a "background" value range. The mean value of 21 µg $m^{-3}$ during SALTRACE is slightly above in this range. Thus measurements made during SALTRACE could be regarded as being representative of "normal" dust conditions.

Figure 4 shows time series of AOD (black crosses) measured with AERONET (AErosol RObotic NETwork, http://aeronet.gsfc.nasa.gov/) sun photometers at Cabo Verde, Barbados and Puerto Rico throughout the main SALTRACE period. It illustrates the dust layer at Barbados with a time-height cross-section of volume linear depolarization ratio (VLDR, for details see discussion of Figure 6). Maximum AOD (500 nm) detected with the sun photometers reached values of 0.85 at Cabo Verde, 0.61 at Barbados and 0.56 at Puerto Rico during SALTRACE. The ground-based lidar measurements at Barbados showed that mineral dust contributed about 50-70% of the total AOD at 532 nm (Groß et al., 2015). The red triangles in Figure 4 indicate the median AOD (500 nm) during the 3-4 hour duration of the individual Falcon flights which fell into the range 0.5-0.8 for flights in the Cabo Verde area and 0.1-0.5 for flights in the Caribbean. The Angstrom exponent of the AOD at the Barbados site (not shown) was around 0.2 on most days except for very clean (dust-free) days where it increased to 0.5.

Most Falcon flights were performed during high-dust concentration conditions, but some flights also focused on low-dust conditions. Figure 4 shows surface-level dust mass concentration at Ragged Point (blue dots) (see Kristensen et al., 2016 for more details on ground-based measurements during SALTRACE). The dust mass concentration was derived from spectral absorption coefficients measured with a Spectral Optical Absorption Photometer (SOAP, Müller et al., 2009) by fitting spectral mass absorption coefficients between wavelengths 425 and 675 nm to the measurements following a reanalysis of data from Müller et al. (2009) and Schladitz et al. (2009).

The temporal trends of AOD and dust concentration at the ground agree well indicating that: (1) dust makes a major contribution to the AOD in the Caribbean; (2) dust transported at higher altitudes into the Caribbean in the SAL is effectively mixed down into the boundary layer over Barbados; and (3) we can expect good comparability between ground-based,

248 airborne and remote sensing observations (see also Figure 12). Previously, Smirnov et al.
249 (2000) had shown that monthly means of AOD and ground-based dust concentrations were
250 highly correlated at Barbados. Our results show a good correlation on a daily basis.

251 **4. Dust source activity during SALTRACE**

252 Various sources across North Africa contribute to the dust load in the Caribbean. Figure 5
253 summarizes the most active dust sources for SALTRACE, SAMUM-1, and SAMUM-2. The Dust
254 source activity (DSA) was inferred from infrared dust index images calculated from brightness
255 temperature measurements by the Spinning Enhanced Visible and Infra-Red Imager (SEVIRI)
256 onboard the Meteosat Second Generation (MSG) satellite (Schepanski et al., 2007; 2009;
257 2012). For each of the three field campaigns, daily maps of DSA were summarized and
258 occurrence frequencies of DSA were calculated (Figure 5). Areas showing a DSA frequency
259 above the 97$^{th}$ percentile for the corresponding time period were colored. The gray-shaded
260 areas indicate all source regions which were active during SALTRACE. Although seasonal and
261 thus campaign-related differences in the pattern distribution of frequent DSA are apparent,
262 dust sources located in the Adrar-Hoggar-Air mountain region as well as the Bodélé
263 Depression region were predominantly active throughout all three campaigns. Dust source
264 hotspots over the northern part of the Sahara and the Maghreb region were predominantly
265 active during SAMUM-1 (May/June) and SALTRACE (June/July) suggesting that these regions
266 are of additional importance in late spring and early summer.

267 Dust from the most active sources during SALTRACE identified in Figure 5 is expected to have
268 a high kaolinite and low illite abundance, as well as low calcium and high total iron contents
269 (Scheuvens et al., 2013; Nousiainen and Kandler, 2015). The ratio of oxide to total iron is
270 estimated to be higher for Bodélé and Hoggar than for Mali sources (Formenti et al., 2014). In

contrast, the less active sources in the northern Sahara would be dominated by illite and exhibit higher calcite contents. Except for Bodélé, the most active sources have a generally high iron oxide content. The dust therefore is expected to contribute considerably to shortwave radiation absorption. It is particularly expected to dominate absorption for super-micron particles (Müller et al., 2009). Furthermore, their comparatively high feldspar content (Nickovic et al., 2012) might influence the specific ice nucleation ability (Atkinson et al., 2013).

## 5. The big picture: mineral transport from Africa into the Caribbean

The large scale features of dust transport from Africa across the Atlantic were initially described in the early 1970s (Prospero et al., 1970; Carlson and Prospero, 1972; Schütz, 1980), but the modification of dust properties during long-range transport is still an open question. After emission over Africa, the warm, dry and dust-containing SAL leaves the African continent and travels westward at a speed of about 1000 km $d^{-1}$, crossing to Barbados in about five days (e.g. Huang et al., 2010). Within the course of the year, the main transport corridor for the dust outflow from Africa exhibits a south-north migration related to the seasonal displacement of the Hadley cell in general and the cycle of the complex West African circulation in particular, in which the African easterly jet and its disturbances, so-called African easterly waves (AEWs), play an important role (e.g. Thorncroft and Blackburn, 1999; Kiladis et al., 2006; Knippertz and Todd, 2010). In June/July, the center of the dust corridor and the largest AOD is found between 15°N and 20°N transporting mineral dust into the Caribbean and towards Florida, whereas in winter, the dust corridor is centered between 5°N and 10°N and the dust extends to South America (Schütz, 1980; Huang et al., 2010; Yu et al., 2015).

As visible in Figure 4, dust concentrations in Barbados have a pulsating nature which is connected to the passage of AEWs (Carlson and Prospero, 1972) which periodically interrupt

294 the dust flow into the Caribbean and occasionally intensify into tropical cyclones (Zipser et al.,
295 2009). The passage of AEWs is associated with moist air, cloudiness and precipitation. Dust
296 events appear to follow behind AEWs (Karyampudi and Carlson, 1988).

297 The structure and vertical distribution of the mineral dust layer changes during transit. Figure
298 6 (top panel) shows these changes by means of cross-sections of backscatter from the
299 airborne wind lidar system onboard the Falcon (Chouza et al., 2015; Chouza et al., 2016a). The
300 bottom panel of Figure 6 sketches the changes in dust layer structure and also the processes
301 modifying the size distribution of the dust aerosol. Over West-Africa, dust extends from the
302 surface to 6-7 km altitude (e.g. Schütz, 1980; Weinzierl et al., 2009). When leaving the African
303 continent, the dust-containing continental outflow over-rides the cool dust-free trade winds
304 to form the elevated SAL (Weinzierl et al., 2009; Weinzierl et al., 2011; Khan et al., 2015). In
305 the Cabo Verde region, the lidar shows a homogenous dust layer extending above the trade-
306 wind inversion from about 1.5 km to 6-7 km altitude (Figure 6, top panel). During transit, the
307 top of the SAL descends from 6-7 km over West Africa to 4-5 km in the Caribbean with an
308 average of ~0.4-0.6 km $d^{-1}$. Dust is transferred from the SAL to the marine boundary layer by
309 entrainment at the top of the marine boundary layer, via turbulent and convective downward
310 mixing, and by gravitational settling of mainly super-micron particles leading to changes in the
311 dust size distribution. In addition, cloud processing, dilution, and wet deposition are expected
312 to modify aerosol properties in the SAL in the course of transport.

313 The vertical layering described in Figure 6 is typical for summer. Figure 7 illustrates the
314 variability and seasonal differences in vertical structure based on ground-based lidar BERTHA
315 (Haarig et al., 2016b; Haarig et al., 2016a) from TROPOS Leipzig at three different locations
316 between Africa and the Caribbean in summer 2006, 2008, 2013 and 2014 and in winter 2008
317 and 2014. The six panels depict time-altitude cross-sections of the volume linear

depolarization ratio (VLDR) at a wavelengths of 710 and 1064 nm, respectively. The VLDR is derived from the ratio of the measured cross- to co-polarized component in the backscattered light when linearly polarized light is emitted by the laser. This quantity includes the contribution from both, molecules and particles. From the VLDR the linear depolarization ratio of particles (PLDR) can be derived which serves to identify aerosol types (e.g. Tesche et al., 2009; Tesche et al., 2011; Weinzierl et al., 2011; Burton et al., 2012; Groß et al., 2013). Regions with predominantly aspherical particles of pure dust (PLDR of 31 ± 3% at 532 nm; Freudenthaler et al., 2009) appear in red. Marine aerosol with mostly spherical particles (PLDR of 2 ± 1% at 532 nm for relative humidities > 50%; Groß et al., 2011) are shown in blue. Mixtures of dust particles with spherical particles (e.g. marine aerosol at high relative humidity, but also biomass particles) appear as yellow-greenish colors (Tesche et al., 2009).

In all cases, the aerosol layers extend from the ground up to altitudes between 3 and 5 km. However, the layer structures change with season because of variations in aerosol types and meteorological conditions, notably the south-north migration of the main transport corridor for the dust and biomass-burning outflow from Africa. In winter, dust is typically transported below 2 km altitude while biomass-burning dust mixtures are carried aloft; transport is primarily in latitudes south of Barbados which receives little aerosol during that time of year. In summer, the vertical aerosol distribution over Barbados shows three layers with different aerosol properties: (1) the boundary layer from the surface up to about 700 m where marine aerosols dominate; (2) above that, a layer of mixed mineral dust and marine aerosols reaching up to 1.5-2.5 km - this also is the height range where (mainly) trade wind cumulus clouds are present; (3) the top layer extends from 1.5-2.5 km to typically 4-5 km and is characterized by relatively pure Saharan dust. This layer contributes about half of the total optical depth at 532 nm (Groß et al., 2015).

Although we describe the trans-Atlantic dust transport in simple terms, it should be clear that the processes are quite complex. Note for example that at Cabo Verde during summer, when transport to the Caribbean is at a maximum, there is very little dust in the marine boundary layer which is dominated by the low-level northeasterly trade wind flow. Transport takes place in the SAL above the measurement site. Similarly at Barbados in summer, the VLDR product would suggest that there is little dust in the boundary layer despite the fact that about 10-40 µg $m^{-3}$ of dust (Figure 4) are present (for comparison: 50 µg $m^{-3}$ is the limit value for 24h-exposure to fine particulate matter (PM10) in the EU, http://ec.europa.eu/environment/air/quality/standards.htm). This is a consequence of the boundary layer being heavily loaded with sea-salt aerosol thus lowering the dust contribution to the total aerosol volume to about 30-40% (Groß et al., 2016) and thereby decreasing the PLDR impact of dust.

## 6. Highlighted SALTRACE results

In this section, we highlight three results from SALTRACE: the first example investigates the modification of mineral dust during trans-Atlantic transport on the basis of a Lagrangian dust sampling experiment between Cabo Verde and Barbados. The second example presents the SALTRACE measurements during the passage of tropical storm Chantal. The third example shows vertical profiles of lidar and *in-situ* parameters for a case with high and low dust loads and discusses the SAL as a reservoir for CCN.

### Modification of dust during transport across the Atlantic Ocean – A Lagrangian case study

One major objective of SALTRACE was to study the "aging" of dust during long-range transport and its impact on the radiation budget and cloud-microphysical processes. This could be

achieved by statistically comparing dust properties measured on the eastern Atlantic and later on the western Atlantic, or by a *Lagrangian experiment* in which the same air mass is sampled multiple times on its trajectory as determined by means of meteorological models.

During SALTRACE we performed a Lagrangian experiment that studied dust in the Cabo Verde region and five days later in the Western Atlantic. We started with a series of north-south tracks in the Cabo Verde area on 17 June 2013. Flight legs at four different altitudes between 1 and 5 km were performed between the islands Sal and Santiago, a distance of 210 km, roughly perpendicular to the dust outflow from the African continent. Before and after the flight, we ran trajectory and dispersion simulations with the Lagrangian dispersion model HYSPLIT (Draxler and Hess, 1998) to predict when the sampled air would arrive over Barbados. This was determined to be on 22 June 2013. In the Caribbean, we carried out two flights on 20 and 21 June 2013, prior to the arrival of the Lagrangian-selected air mass. We performed the Lagrangian flight on 22 June 2013 where we flew on a north-south track along 59.5°W, i.e. perpendicular to the direction of propagation of the dust layer from Africa to the Caribbean. The flight included several overpasses over Barbados at altitudes between 0.3 and 9 km, and extended over a distance of ~470 km between 10.4°N and 14.6°N. According to post-campaign analyses, the air mass sampled on 17 June 2013 at an altitude of 2.6 km in the Cabo Verde region was again sampled on 22 June 2013 over Barbados at an altitude of 2.3 km. It was above the typical scattered cloud layer extending from ~0.7 to 2 km on that day.

The Lagrangian experiment relies on a certain degree of homogeneity of the sampled air mass, a precondition which is satisfied by the well-mixed SAL. For example, the variability of the particle number concentration in the Lagrangian leg over Cabo Verde was below ~10% in the coarse mode (0.5-50 µm) and below ~20% in the accumulation mode (80-310 nm) over distances of more than 180 km.

Figure 8 visualizes the air mass transport of the Lagrangian experiment on the basis of COSMO-MUSCAT (COSMO: Consortium for Small-scale Modelling; MUSCAT: MUltiScale Chemistry Aerosol Transport Model) simulations. COSMO-MUSCAT is a regional dust model system which computes the size-resolved distribution of Saharan dust including radiative effects and feedbacks (Heinold et al., 2007; Heinold et al., 2011). Simulations were run for the period April to July 2013 with 28 km horizontal grid spacing on a model domain that covers the Saharan desert and the tropical Atlantic Ocean including the Caribbean. Combined with trajectory analysis, COSMO-MUSCAT shows the relationship between the sampling areas at Cabo Verde and Barbados. According to these simulations, the predominant number of trajectories launched over Cabo Verde arrived at Barbados within a 250-km radius within the five days transport time.

The four panels in Figure 8 illustrate the location and extent of the dust layer sampled on both sides of the Atlantic in the Lagrangian experiment as it crosses the Atlantic Ocean. Color-coded dust AOD maps are combined with longitude-altitude cross-sections through the dust layer which show model dust mass concentrations on 17, 18, 20 and 22 June 2013. The position and timing of maps and cross-sections exactly correspond to the course of a 7-day forward trajectory starting over Cabo Verde (23.3°W/15.5°N) on 17 June 2013, and computed with COSMO wind fields. During transport, the modeled dust layer depth decreases from about 5 km (Cabo Verde) to 4 km (Barbados area) and about half of the dust mass is removed. AERONET measurements in Cabo Verde and Barbados confirm a decrease in the AOD (500 nm) by a factor of about two from 0.54 to 0.26 within the five days. Similar results were obtained from the long-range transport study carried out based on the airborne Doppler wind lidar retrievals and model results of MACC (Monitoring Atmospheric Composition and Climate), the global aerosol model from European Centre for Medium-Range Weather Forecasts (Chouza et

al., 2016a). Although MACC was able to reproduce the general characteristics of the dust long-range transport process, important differences were observed in the dust vertical distribution and the African Easterly Jet intensity.

Figure 9 shows aerosol size distributions detected in Cabo Verde (blue symbols) at an altitude of 2.6 km and the corresponding measurements made five days later at an altitude of 2.3 km over Barbados (red symbols). The size distribution includes the total aerosol in the SAL and was detected with a combination of a condensation particle counter (CPC) and several optical particle counters (OPC). Detailed information about instruments used is given in Table 3 in the supplemental material. Data from the CPC, the Grimm Sky OPC, and the Ultra Sensitivity Aerosol Spectrometer (UHSAS-A) were inverted with a consistent Bayesian inversion procedure and parameterized assuming three log-normal distributions following the method described following the method described in Walser et al. (2016). The uncertainty range in the submicron size range reflects the uncertainty in the lognormal size distribution mode parameters. The super-micron size range was detected with a Cloud and Aerosol Spectrometer with Depolarization Detection (CAS-DPOL). The shaded areas indicate the 10 and 90 percentile concentration values from the CAS-DPOL spectrometer. The complete size distribution (sub- and super-micron range) was parameterized with four log-normal distributions (solid lines).

Although in particular the coarse mode aerosol size range is associated with considerable uncertainties, changes are clearly visible in both, total particle number concentration and number size distribution. With respect to particle number concentration in the size range between 10 nm and 50 µm, about 49% of all particles are “lost” during trans-Atlantic transport. The number fraction of removed particles is size-dependent and increases with increasing particles size. For example, in the size range between 1 and 10 µm about 60% of

436 the particles are removed whereas 80% of the 20 µm particles and 90% of the 30 µm particles
437 are gone suggesting that dry deposition is the dominating removal process at least during this
438 case.

439 The detection of 20-30 µm particles in the Caribbean even after more than 4000 km and five
440 days of transport is unexpected. Although Maring et al. (2003) pointed out that Stokes
441 gravitational settling overestimated the removal of particles < 7.3 µm, they found that larger
442 particles were effectively removed between Tenerife and Puerto Rico. In contrast, Denjean et
443 al. (2016) found that the modal peak diameter of the volume size distribution remained
444 unvaried from one side to the other of the Atlantic Ocean (i.e. Cabo Verde to Puerto Rico)
445 suggesting that after 2-3 days from uplift gravitational settling is practically ineffective.
446 Assuming a density of 2.6 g $cm^{-3}$ for dust and a shape factor of 1.4 (Hinds, 1999) to account
447 for the non-spherical particle shape which slows down the settling velocity, a particle with
448 20 µm (30 µm) in diameter descends 2.1 km (4.6 km) per day. This means that even if 20 µm
449 (30 µm) particles had been at the top of the SAL at an altitude of 6-7 km over Cabo Verde,
450 they should have been removed from the atmosphere within three days (1.5 days). The
451 Barbados measurements shown in Figure 9 were performed at 2.3 km altitude above ground
452 and about 1.3 km below the SAL top. Assuming SAL transport without vertical shear, and thus
453 a Stokes settling distance of 1.3 km for this measurement, the expected maximum particle
454 size would be about 7 µm. In contrast, 20% (10%) of the 20 µm (30 µm) survived in the dust
455 layer and were observed over Barbados after five days of transport (Figure 8), a fact which
456 may have important implications for the dust radiative effects and the ability of particles to
457 act as INP. To understand the presence of these super-micron particles, Gasteiger et al. (2016)
458 investigated particle settling in the SAL from an integrated model, lidar, and in-situ
459 perspective. Although not claiming that their simplified model describes processes during

460 long-range transport in detail, their model suggests that day-time convective mixing within
461 the SAL would allow a fraction of particles with diameters of 20 µm and larger to arrive in the
462 Caribbean.

463 During SALTRACE, we sampled particles onboard the Falcon for offline-chemical analyses. For
464 the Lagrangian case, approximately 3000 particles were collected. These were analyzed by
465 scanning electron microscopy and energy-dispersive X-ray diffraction (EDX) for size and
466 composition, and by transmission electron microscopy and EDX for volatility and composition.
467 Particles were classified according to the chemical composition as described in Kandler et al.
468 (2009) with the exception of quartz being classified as silicate. Volatility was determined
469 according to a method previously described (Kandler et al., 2011; Kristensen et al., 2016).

470 Figure 10 shows the aerosol composition and volatility state before and after trans-Atlantic
471 transport for the Lagrangian case. The general composition with comparatively low calcium
472 contents in the super-micron fraction is in line with the mainly southern Saharan/Sahelian
473 sources (Scheuvens et al., 2013). The change in composition at about 500 nm particle size after
474 long-range transport is more pronounced than in the dust-influenced Cabo Verde boundary
475 layer (Kandler et al., 2011; Lieke et al., 2011), but less distinct than observed by chemical and
476 microphysical measurements over the African continent (Kaaden et al., 2009; Kandler et al.,
477 2009; Müller et al., 2009; Weinzierl et al., 2009).

478 Comparing the chemical composition before and after transport reveals an increase in the
479 number abundance of soluble sulfates – most ammonium- and sodium-dominated sulfates –
480 for submicron particles; also, there is a slightly increased abundance of particles internally
481 mixed between silicate and sulfate. This is corroborated by the fact that the abundance of
482 silicate particles with detectable amounts of sulfate (approx. 1 %) increased from 2.5 % to

4.3 %. For super-micron particles, no considerable modification is visible, which is consistent with other recent observations in the Caribbean (Denjean et al., 2015). Also, the relative composition of the dust component with respect to different silicates (not shown) is indistinguishable before and after transport.

The volatility experiment for submicron particles reveals, in contrast, that there is an increase in both the amount of volatile material on the single particles and the abundance of totally volatile particles. The lower panel of Figure 10 shows the composition of the refractory residuals. Here, there is a clear increase in soot whereas dust decreases. Refractory material classified as “other” consists mainly of iron (probably oxides/hydroxides) and K-rich particles (perhaps biomass burning material) (Lieke et al., 2011). The median volume fraction of volatile material internally mixed with soot is higher in transported aerosol (89 % versus 79 %). This volatile volume fraction for internally-mixed dust particles does not change (7 % versus 8 %).

**The passage of tropical storm Chantal and its impact on the Saharan Air Layer**

During SALTRACE, we had the unique opportunity to perform extended aerosol measurements before, during and after the passage of tropical storm Chantal which evolved in a SAL environment. The SAL is attracting great interest because it is suspected to influence tropical cyclone activity (e.g. Dunion and Velden, 2004; Evan et al., 2011). The observed modulation of the tropical Atlantic cyclone activity in the presence of the SAL has been attributed to various causes. Evan et al. (2011) link weak cyclone activity to surface cooling through the radiative effects of the dust particles in the SAL. Furthermore, dust particles acting as CCN and INP might influence the development and formation of precipitation in the convective clouds and thus impact on the cyclone development. Local vertical wind shear can

505 be enhanced by the midlevel jet found in the SAL, thereby hindering cyclone development
506 (Dunion and Velden, 2004).

507 Figure 11 (top panel) shows a time series of VLDR and range corrected backscatter for the
508 period between 8 and 11 July 2013 detected with the LMU lidar system POLIS (Freudenthaler
509 et al., 2016) together with a map of the Meteosat SAL-tracking satellite product which we
510 overlaid with contours of dust AOD from simulations with the regional Saharan dust model
511 COSMO-MUSCAT. Both observations and regional dust simulations show that the passage of
512 Chantal was associated with a reduced dust load in the Caribbean which may largely be caused
513 by mixing in clean air from further south but also by wet removal of aerosols. This change in
514 air mass is obvious from the SAL-tracking product (Figure 11, bottom panel), while the analysis
515 of dust model results including and without the storm event (not shown) reveals a minor role
516 of wet deposition in the removal of dust. Vertical mixing was enhanced especially to the rear
517 of the cyclone. Immediately after the passage of Chantal, changes in the dust properties were
518 observed (Figure 12) which might be linked to a change in the large-scale flow pattern over
519 the tropical North Atlantic and West Africa causing increased dust transport from southern
520 Saharan and Sahelian dust sources. The dust layer was seen to extend to about 5 km, higher
521 than the typically observed 4-5 km. Details about DSA over North Africa and transported dust
522 reaching Barbados are given in Groß et al. (2015). Future investigations will focus on the
523 interactions of tropical storm Chantal and dust transport, including sensitivity studies on dust
524 radiative effects and feedbacks on atmospheric dynamics and sea surface temperature.

525 **The SAL as a reservoir/source for CCN**

526 Here we highlight the vertical distribution of the microphysical properties of mineral dust, its
527 ability to act as CCN. Mineral particles may serve as CCN in liquid cloud droplet formation

(Sullivan et al., 2009; Garimella et al., 2014), and as such they are likely to be of great importance over the tropical Atlantic (Twohy et al., 2009). The efficacy of dust particles to act as CCN increases significantly with particle size, but it is also influenced by the presence of coatings and the amount of (water soluble) coating material (e.g. Garimella et al., 2014). Pure mineral dust particles are hydrophobic, but if they are larger than ~0.4-0.8 µm they will act as CCN at atmospherically relevant supersaturations (Sullivan et al., 2009; Garimella et al., 2014). The addition of even minor amounts of water soluble material will increase the potential of dust particles to act as CCN (Sullivan et al., 2009). Furthermore, the addition of soluble material onto dust particles increases the water uptake at sub-saturated conditions with respect to liquid water (Hatch et al., 2008), and thus influences their optical properties and the ability to scatter/absorb radiation.

Consequently, to assess the direct and indirect climate impacts from mineral particles, it is essential to investigate their mixing state and how that could change as the particles age in the atmosphere. Some studies indicate that processing of dust in the atmosphere leads to an addition of water soluble material (e.g. Perry et al., 2004; Begue et al., 2015). However, there have been only few studies of the properties of aged African dust transported across the Atlantic. Denjean et al. (2015) investigated super-micron mineral dust particles sampled in Puerto Rico. They reported that up to 24% of the studied mineral dust particles were internally mixed with sulfate or chloride, while 3-6% formed aggregates with sea-salt particles. Only the latter group of mineral particles showed increased hygroscopic growth for relative humidity up to 94%.

Ground-based and airborne direct measurements of CCN concentrations were performed during SALTRACE. The potential of polarization lidar data to estimate vertical profiles of cloud-relevant aerosol parameters (CCN and INP number concentrations) was explored (Mamouri

552 and Ansmann, 2015). Furthermore, samples were collected for off-line analysis of hygroscopic
553 growth and ice nucleation ability.

554 Figure 12 contrasts vertical profiles of aerosol number concentration in different size classes
555 together with extinction coefficient measured with the ground-based lidar system from LMU
556 Munich for days with high (11 July 2013) and low (8 July 2013) dust concentrations in
557 Barbados. In addition, vertical profiles of PLDR enable us to distinguish the SAL pure dust layer
558 which extends above about 1.5 km (8 July) and 1.8 km (11 July), respectively, from the marine
559 aerosol-dust mixture in the marine mixed layer. The particle number concentration in the fine
560 mode (10 nm – 60 nm) seems to be depleted inside the SAL, while accumulation (60 nm –
561 1 µm) and coarse mode (0.5 – 50 µm) is enhanced by a factor of more than 4 and 15,
562 respectively, compared to free-tropospheric concentrations in these size ranges. The vertical
563 profile of the CCN number concentration is correlated with accumulation and coarse mode
564 number concentration. On the day with high dust loads, the CCN number concentration at
565 altitudes of ~2-4 km is enhanced by a factor of about 5 compared to the day with the low dust
566 load. Hence, it is likely that properties of clouds in the Caribbean formed at those altitudes are
567 significantly influenced by long-range transported particles from Northern Africa.

568 **7. Summary and outlook**

569 Although it is generally accepted that mineral dust affects many climate processes, our
570 understanding of long-range transported dust is limited by the fragmentary nature of past
571 studies. The strategy of SALTRACE was to attain a large-scale picture of African dust transport
572 across the Atlantic by linking ground-based and airborne measurements with remote sensing
573 and modeling. Specific objectives were: (1) to characterize the chemical, microphysical and
574 optical properties of “aged” dust in the Caribbean, (2) to quantify the impact of dust “aging”

on the radiation budget and cloud-microphysical processes, (3) to investigate the meteorological context of African dust transport into the Caribbean, and (4) to assess the roles of removal processes during transport.

The SALTRACE program in 2013 – 2014, especially with the aircraft field experiment in June/July 2013, comprised by far the most extensive measurements ever performed to study long-range transported dust. To our knowledge, the Lagrangian in-situ study which sampled coherent air masses separated by a distance of more than 4,000 km was unique and enables a detailed investigation of transport effects on dust properties.

The Lagrangian results were surprising in that they suggest that the removal rate of large super-micron particles is slower than expected and the chemical alterations to the particles are less pronounced than expected. The exact nature of these aging processes is unclear and more research will be needed. The SALTRACE data set enables future studies to look in detail at changes of chemical, microphysical and optical dust properties during transport and quantify their associated effects on radiation and clouds.

To place the SALTRACE measurements in a long-term context we related our measurements to the 50-year Barbados dust record and found that the situation investigated during SALTRACE can be regarded as “normal” dust conditions. Thus the SALTRACE data set is well-suited to constrain the Atlantic and Caribbean dust properties and concentrations in models. Temporal trends of ground-based dust mass concentrations and AOD at Barbados agreed well with aircraft measurements indicating that (1) mineral dust makes a significant contribution to the AOD in the Caribbean, (2) dust transported at higher altitudes into the Caribbean is effectively mixed down into the boundary layer, and (3) that in general we can expect good comparability between ground-based, airborne and remote sensing observations.

598 We carried out extensive measurements in tropical storm Chantal which developed when dust
599 concentrations were high over broad areas of the western Atlantic. Chantal passed through
600 the Barbados region on 9 July 2013. Interestingly, by the time the storm over-passed our
601 ground-site on Barbados essentially all dust was gone, an observation which we attribute to
602 enhanced advection of dust-free air from the south. The SAL-tracking product
603 and modeled dust AOD in Figure 11 clearly show this change in air mass associated with the
604 passage of storm Chantal.

605 We collected numerous in-situ and remote sensing profiles of dust properties which we
606 evaluated with respect to their ability to act as CCN. We found the CCN number concentration
607 in the SAL to be highly enhanced (~up to a factor of 5) under conditions of high dust loads
608 compared to low dust loads.

609 The SALTRACE data should yield new insights on the formation (and destruction) of the dust-
610 bearing SAL and its impact on cloud evolution processes, the atmospheric radiation budget,
611 and local meteorology. Ongoing analyses are expected to elucidate details on the processes
612 occurring at the end of the atmospheric dust cycle as the SAL moved over the Caribbean.

613 Simultaneous Doppler lidar backscatter and wind measurements were conducted for the first
614 time along the main Saharan dust transport path. This unique dataset not only provides the
615 opportunity to investigate various features associated with this transport, but also to test the
616 ability of different global and regional models to simulate them. Ongoing regional modeling
617 will use the rich data set to address fundamental questions on Saharan dust transport: how
618 export across the tropical Atlantic is influenced by the West African circulation; the role played
619 by the different removal and mixing processes; and the impact of dust on radiative forcing on

620 the dynamics of the SAL. Regional dust simulations and trajectory analysis will be used to
621 explore deposition processes, particle aging, and dust-cloud interactions.

622 The role of dust as CCN and INP and the associated impacts on weather needs further
623 research. The next generation of mineral dust field experiments should focus on extended
624 characterization of dust aerosol and include enhanced cloud observations (e.g., mixed phase
625 and ice clouds developing in dusty air layers) by combined in-situ and remote sensing
626 observations.

627 Finally, the long-term dust record from Barbados shows that large changes in transport have
628 occurred and that these are clearly linked to climate in ways that we do not fully understand.
629 In the coming decades we might expect continuing changes in global climate. However the
630 projections for North Africa are highly uncertain and we cannot anticipate whether dust
631 transport will increase or decrease (Seneviratne et al., 2012). Thus it is important that dust
632 transport out of Africa is carefully monitored in the coming years to better understand the
633 controlling processes so as to develop better model projections of dust transport and the role
634 of dust in a changing climate.

635 **8. Acknowledgements**

636 The research leading to these results has received funding from the Helmholtz Association
637 under grant number VH-NG-606 (Helmholtz-Hochschul-Nachwuchsforschergruppe AerCARE)
638 and from the European Research Council under the European Community's Horizon 2020
639 research and innovation framework program/ERC grant agreement No. 640458 (A-LIFE). The
640 SALTRACE campaign was mainly funded by the Helmholtz Association, DLR, TROPOS, and LMU.
641 The SALTRACE flights in the Cabo Verde region were funded through the DLR-internal project
642 VolcATS (Volcanic ash impact on the Air Transport System). We acknowledge funding from the

643 LMU Munich's Institutional Strategy LMUexcellent within the framework of the German
644 Excellence Initiative. The photometer calibration was supported by European Union's Horizon
645 2020 research and innovation programme under grant agreement No 654109 (ACTRIS-2). J.
646 M. Prospero's research is supported by NSF grant AGS-0962256. K. Kandler acknowledges
647 financial support from the German Research Foundation (DFG, grants KA 2280/2 and FOR
648 1525 INUIT). T. B. Kristensen thanks for funding from the German Federal Ministry of
649 Education and Research (BMBF) project 01LK1222B.

650 We thank the SALTRACE team and our local hosts for their support and the great collaboration.
651 We are grateful to DLR flight experiments, in particular Andrea Hausold and Frank Probst, the
652 pilots Stefan Grillenbeck, Michael Großrubatscher, Philipp Weber, Roland Welser, and the
653 technical and sensor team from DLR flight operations for their great support during the
654 preparation of SALTRACE and for the accomplishment of the research flights. Special thanks
655 due to the certification team of CAS-DPOL for enabling us to fly this instrument on the Falcon.
656 We are grateful to the following participants of the SALTRACE field experiment for their
657 assistance before, during, and after the SALTRACE field phase: Reinhold Busen, Florian
658 Dahlkötter, Daniel Fütterer, Markus Hartmann, Katharina Heimerl, André Klepel, Melanie
659 Kujukovic, Christian Lemmerz, Anton Lex, Andreas Minikin, Engelbert Nagel, Stephan Rahm,
660 Maximilian Rose, Meinhard Seefeldner, and Benjamin Witschas. Thanks are due to Andreas
661 Dörnbrack, Robert Baumann and Ingo Wenzel for preparing ECMWF and HYSPLIT trajectories
662 and for their support with the weather forecast during SALTRACE. We thank Didier Tanré and
663 LOA staff for their effort in establishing and maintaining Cabo Verde AERONET site, and the
664 Deutscher Wetterdienst (DWD) for good cooperation and support running the COSMO model
665 and providing the required input data. We are grateful to the NASA CALIPSO team for
666 providing CALIPSO data already three hours after downlink. Matthias Tesche kindly provided

667 the SAMUM-1 and SAMUM-2 data in Fig. 8. We thank the University of Wisconsin – CIMSS for
668 providing the Meteosat SAL-layer tracking product.

669 SALTRACE would not have been possible without the excellent support from local authorities
670 in Cabo Verde and Barbados including the Regional Security System (RSS), the Caribbean
671 Institute for Meteorology and Hydrology (CIMH), and the Airport Authority GAIA (Grantley
672 Adams International Airport Inc.) Barbados who hosted us in their facilities and supported us
673 to get clearances which we gratefully acknowledge.

## References


Abdelkader, M., S. Metzger, R. E. Mamouri, M. Astitha, L. Barrie, Z. Levin, and J. Lelieveld, 2015: Dust–air pollution dynamics over the eastern Mediterranean. *Atmos. Chem. Phys.*, **15,** 9173-9189**,** doi:10.5194/acp-15-9173-2015.

Ansmann, A., A. Petzold, K. Kandler, I. Tegen, M. Wendisch, D. Müller, B. Weinzierl, T. Müller, and J. Heintzenberg, 2011: Saharan Mineral Dust Experiments SAMUM-1 and SAMUM-2: What have we learned? *Tellus*, **63B,** 403-429**,** doi:10.1111/j.1600-0889.2011.00555.x.

Atkinson, J. D., B. J. Murray, M. T. Woodhouse, T. F. Whale, K. J. Baustian, K. S. Carslaw, S. Dobbie, D. O'Sullivan, and T. L. Malkin, 2013: The importance of feldspar for ice nucleation by mineral dust in mixed-phase clouds. *Nature*, **498,** 355-358**,** doi:10.1038/nature12278.

Balkanski, Y., M. Schulz, T. Claquin, and S. Guibert, 2007: Reevaluation of Mineral aerosol radiative forcings suggests a better agreement with satellite and AERONET data. *Atmos. Chem. Phys.*, **7,** 81-95**,** doi:10.5194/acp-7-81-2007.

Begue, N., P. Tulet, J. Pelon, B. Aouizerats, A. Berger, and A. Schwarzenboeck, 2015: Aerosol processing and CCN formation of an intense Saharan dust plume during the EUCAARI 2008 campaign. *Atmos. Chem. Phys.*, **15,** 3497-3516**,** doi:10.5194/acp-15-3497-2015.

Brammer, A., and C. D. Thorncroft, 2015: Variability and Evolution of African Easterly Wave Structures and Their Relationship with Tropical Cyclogenesis over the Eastern Atlantic. *Mon. Weather Rev.*, **143,** 4975-4995**,** doi:10.1175/MWR-D-15-0106.1.

Braun, S. A., 2010: Reevaluating the role of the Saharan air layer in Atlantic tropical cyclogenesis and evolution. *Mon. Weather Rev.*, **138,** 2007-2037**,** doi:10.1175/2009MWR3135.1.

Burton, S. P., R. A. Ferrare, C. A. Hostetler, J. W. Hair, R. R. Rogers, M. D. Obland, C. F. Butler, A. L. Cook, D. B. Harper, and K. D. Froyd, 2012: Aerosol classification using airborne High Spectral Resolution Lidar measurements - methodology and examples. *Atmos. Meas. Tech.*, **5,** 73-98**,** doi:10.5194/amt-5-73-2012.

Carlson, T. N., and J. M. Prospero, 1972: The Large-Scale Movement of Saharan Air Outbreaks over the Northern Equatorial Atlantic. *J. Appl. Met.*, **11,** 283-297.

Chouza, F., O. Reitebuch, A. Benedetti, and B. Weinzierl, 2016a: Saharan dust long-range transport across the Atlantic studied by an airborne Doppler wind lidar and the MACC model. *Atmos. Chem. Phys.*, **16,** 11581-11600**,** doi:10.5194/acp-16-11581-2016.

Chouza, F., O. Reitebuch, M. Jähn, S. Rahm, and B. Weinzierl, 2016b: Vertical wind retrieved by airborne lidar and analysis of island induced gravity waves in combination with numerical models and in situ particle measurements. *Atmos. Chem. Phys.*, **16,** 4675-4692**,** doi:10.5194/acp-16-4675-2016.

707 Chouza, F., O. Reitebuch, S. Groß, S. Rahm, V. Freudenthaler, C. Toledano, and B. Weinzierl, 2015:
708 Retrieval of aerosol backscatter and extinction from airborne coherent Doppler wind lidar
709 measurements. *Atmos. Meas. Tech.*, **8,** 2909-2926**,** doi:10.5194/amt-8-2909-2015.

710 Cotton, R. J., 2016 Ice in Clouds Experiment – Dust: a field campaign to study aerosol-cloud
711 interactions. *96th AMS Annual Meeting*, Amer. Meteor. Soc., J5.3.

712 Dahlkötter, F., M. Gysel, D. Sauer, A. Minikin, R. Baumann, P. Seifert, A. Ansmann, M. Fromm, C. Voigt,
713 and B. Weinzierl, 2014: The Pagami Creek smoke plume after long-range transport to the upper
714 troposphere over Europe - aerosol properties and black carbon mixing state. *Atmos. Chem. Phys.*, **14,**
715 6111-6137**,** doi:10.5194/acp-14-6111-2014.

716 DeFlorio, M. J., I. D. Goodwin, D. R. Cayan, A. J. Miller, S. J. Ghan, D. W. Pierce, L. M. Russell, and B.
717 Singh, 2016: Interannual modulation of subtropical Atlantic boreal summer dust variability by ENSO.
718 *Clim. Dyn.*, **46,** 585-599**,** doi:10.1007/s00382-015-2600-7.

719 Denjean, C., S. Caquineau, K. Desboeufs, B. Laurent, M. Maille, M. Quiñones Rosado, P. Vallejo, O. L.
720 Mayol-Bracero, and P. Formenti, 2015: Long-range transport across the Atlantic in summertime does
721 not enhance the hygroscopicity of African mineral dust. *Geophys. Res. Lett.*, **42,** 7835-7843**,**
722 doi:10.1002/2015gl065693.

723 Denjean, C., F. Cassola, A. Mazzino, S. Triquet, S. Chevaillier, N. Grand, T. Bourrianne, G. Momboisse,
724 K. Sellegri, A. Schwarzenbock, E. Freney, M. Mallet, and P. Formenti, 2016: Size distribution and optical
725 properties of mineral dust aerosols transported in the western Mediterranean. *Atmos. Chem. Phys.*,
726 **16,** 1081-1104**,** doi:10.5194/acp-16-1081-2016.

727 Doherty, O. M., N. Riemer, and S. Hameed, 2008: Saharan mineral dust transport into the Caribbean:
728 Observed atmospheric controls and trends. *J. Geophys. Res.*, **113,** doi:10.1029/2007jd009171.

729 Draxler, R. R., and G. D. Hess, 1998: An overview of the HYSPLIT_4 modeling system of trajectories,
730 dispersion, and deposition. *Aust. Meteor. Mag.*, **47,** 295-308.

731 Dunion, J. P., and C. S. Velden, 2004: The Impact of the Saharan Air Layer on Atlantic Tropical Cyclone
732 Activity. *Bull. Am. Met. Soc.*, **85,** 353-365**,** doi:10.1175/BAMS-85-3-353.

733 Evan, A. T., A. K. Heidinger, and P. Knippertz, 2006: Analysis of winter dust activity off the coast of West
734 Africa using a new 24-year over-water advanced very high resolution radiometer satellite dust
735 climatology. *J. Geophys. Res.*, **111,** D12210**,** doi:10.1029/2005JD006336.

736 Evan, A. T., G. R. Foltz, D. X. Zhang, and D. J. Vimont, 2011: Influence of African dust on ocean-
737 atmosphere variability in the tropical Atlantic. *Nat. Geosci.*, **4,** 762-765**,** doi:10.1038/ngeo1276.

738 Evan, A. T., C. Flamant, M. Gaetani, and F. Guichard, 2016: The past, present and future of African dust.
739 *Nature*, **531,** 493-495**,** doi:10.1038/nature17149.

740 Fitzgerald, E., A. P. Ault, M. D. Zauscher, O. L. Mayol-Bracero, and K. A. Prather, 2015: Comparison of
741 the mixing state of long-range transported Asian and African mineral dust. *Atmosph. Env.*, **115,** 19-25**,**
742 doi:10.1016/j.atmosenv.2015.04.031.

743 Formenti, P., S. Caquineau, K. Desboeufs, A. Klaver, S. Chevaillier, E. Journet, and J. L. Rajot, 2014:
744 Mapping the physico-chemical properties of mineral dust in western Africa: mineralogical composition.
745 *Atmos. Chem. Phys.*, **14,** 10663-10686**,** doi:10.5194/acp-14-10663-2014.

746 Freudenthaler, V., M. Seefeldner, S. Groß, and U. Wandinger, 2016: Accuracy of Linear Depolarisation
747 Ratios in Clean Air Ranges Measured with POLIS-6 at 355 and 532 nm. *EPJ Web of Conferences*, 25013.

748 Freudenthaler, V., M. Esselborn, M. Wiegner, B. Heese, M. Tesche, A. Ansmann, D. Müller, D.
749 Althausen, M. Wirth, A. Fix, G. Ehret, P. Knippertz, C. Toledano, J. Gasteiger, M. Garhammer, and M.
750 Seefeldner, 2009: Depolarization ratio profiling at several wavelengths in pure Saharan dust during
751 SAMUM 2006. *Tellus*, **61B,** 165-179**,** doi:10.1111/j.1600-0889.2008.00396.x.

752 Garimella, S., Y. W. Huang, J. S. Seewald, and D. J. Cziczo, 2014: Cloud condensation nucleus activity
753 comparison of dry- and wet-generated mineral dust aerosol: the significance of soluble material.
754 *Atmos. Chem. Phys.*, **14,** 6003-6019**,** doi:10.5194/acp-14-6003-2014.

755 Gasteiger, J., S. Groß, B. Weinzierl, D. Sauer, and V. Freudenthaler, 2016: Particle settling and
756 convective mixing in the Saharan Air Layer as seen from an integrated model, lidar, and in-situ
757 perspective. *Atmos. Chem. Phys. Discuss.*, **2016,** 1-23**,** doi:10.5194/acp-2016-480.

758 Ginoux, P., J. M. Prospero, O. Torres, and M. Chin, 2004: Long-term simulation of global dust
759 distribution with the GOCART model: correlation with North Atlantic Oscillation. *J. Environ. Model.*
760 *Software* **19,** 113-128**,** doi:10.1016/S1364-8152(03)00114-2.

761 Gioda, A., O. L. Mayol-Bracero, F. N. Scatena, K. C. Weathers, V. L. Mateus, and W. H. McDowell, 2013:
762 Chemical constituents in clouds and rainwater in the Puerto Rican rainforest: Potential sources and
763 seasonal drivers. *Atmosph. Env.*, **68,** 208-220**,** doi:10.1016/j.atmosenv.2012.11.017.

764 Goudie, A. S., 2014: Desert dust and human health disorders. *Environ. Int.*, **63,** 101-113**,**
765 doi:10.1016/j.envint.2013.10.011.

766 Groß, S., M. Esselborn, B. Weinzierl, M. Wirth, A. Fix, and A. Petzold, 2013: Aerosol classification by
767 airborne high spectral resolution lidar observations. *Atmos. Chem. Phys.* , **12,** 25983-26028**,**
768 doi:10.5194/acp-13-2487-2013.

769 Groß, S., V. Freudenthaler, K. Schepanski, C. Toledano, A. Schäfler, A. Ansmann, and B. Weinzierl, 2015:
770 Optical properties of long-range transported Saharan dust over Barbados as measured by dual-
771 wavelength depolarization Raman lidar measurements. *Atmos. Chem. Phys.*, **15,** 11067-11080**,**
772 doi:10.5194/acp-15-11067-2015.

773 Groß, S., J. Gasteiger, V. Freudenthaler, T. Müller, D. Sauer, C. Toledano, and A. Ansmann, 2016:
774 Saharan dust contribution to the Caribbean summertime boundary layer – a lidar study during
775 SALTRACE. *Atmos. Chem. Phys.*, **16,** 11535-11546**,** doi:10.5194/acp-16-11535-2016.

776 Groß, S., M. Tesche, V. Freudenthaler, C. Toledano, M. Wiegner, A. Ansmann, D. Althausen, and M.
777 Seefeldner, 2011: Characterization of Saharan dust, marine aerosols and mixtures of biomass burning
778 aerosols and dust by means of multi-wavelength depolarization- and Raman measurements during
779 SAMUM-2. *Tellus*, **63B,** 706-724**,** doi:10.1111/j.1600-0889.2011.00556.x.

780 Haarig, M., D. Althausen, A. Ansmann, A. Klepel, H. Baars, R. Engelmann, S. Groß, and V. Freudenthaler,
781 2016a: Measurement of the Linear Depolarization Ratio of Aged Dust at Three Wavelengths (355, 532
782 and 1064 nm) Simultaneously over Barbados. *EPJ Web of Conferences*, 18009.

783 Haarig, M., D. Althausen, A. Ansmann, R. Engelmann, H. Baars, A. Klepel, S. Groß, V. Freudenthaler, S.
784 P. Burton, E. Marinou, and J. Gasteiger, 2016b: Triple-wavelength depolarization-ratio profiling with
785 lidar in Saharan dust over Barbados during SALTRACE 2013 and 2014. *Atmos. Chem. Phys.*, in
786 preparation.

787 Hankes, I., Z. Wang, G. Zhang, and C. Fritz, 2015: Merger of African easterly waves and formation of
788 Cape Verde storms. *Q. J. R. Meteorol. Soc.*, **141,** 1306-1319**,** doi:10.1002/qj.2439.

789 Hatch, C. D., K. M. Gierlus, J. D. Schuttlefield, and V. H. Grassian, 2008: Water adsorption and cloud
790 condensation nuclei activity of calcite and calcite coated with model humic and fulvic acids. *Atmosph.*
791 *Environ.*, **42,** 5672-5684**,** doi:10.1016/j.atmosenv.2008.03.005.

792 Haywood, J. M., B. T. Johnson, S. R. Osborne, A. J. Baran, M. Brooks, S. F. Milton, J. Mulcahy, D. Walters,
793 R. P. Allan, A. Klaver, P. Formenti, H. E. Brindley, S. Christopher, and P. Gupta, 2011: Motivation,
794 rationale and key results from the GERBILS Saharan dust measurement campaign. *Q. J. R. Meteorol.*
795 *Soc.*, **137,** 1106-1116**,** doi:10.1002/qj.797.

796 Haywood, J. M., J. Pelon, P. Formenti, N. Bharmal, M. Brooks, G. Capes, P. Chazette, C. Chou, S.
797 Christopher, H. Coe, J. Cuesta, Y. Derimian, K. Desboeufs, G. Greed, M. Harrison, B. Heese, E. J.
798 Highwood, B. Johnson, M. Mallet, B. Marticorena, and Coauthors, 2008: Overview of the Dust and
799 Biomass-burning Experiment and African Monsoon Multidisciplinary Analysis Special Observing
800 Period-0. *J. Geophys. Res.*, **113,** D00C17**,** doi:10.1029/2008jd010077.

801 Heinold, B., J. Helmert, O. Hellmuth, R. Wolke, A. Ansmann, B. Marticorena, B. Laurent, and I. Tegen,
802 2007: Regional modeling of Saharan dust events using LM-MUSCAT: model description and case
803 studies. *J. Geophys. Res.*, **112,** D11204**,** doi:10.1029/2006JD007443.

804 Heinold, B., I. Tegen, K. Schepanski, M. Tesche, M. Esselborn, V. Freudenthaler, S. Gross, K. Kandler, P.
805 Knippertz, D. Müller, A. Schladitz, C. Toledano, B. Weinzierl, A. Ansmann, D. Althausen, T. Müller, A.
806 Petzold, and A. Wiedensohler, 2011: Regional modelling of Saharan dust and biomass-burning smoke
807 Part I: Model description and evaluation *Tellus*, **63B,** 781-799**,** doi:10.1111/j.1600-0889.2011.00570.x.

808 Heintzenberg, J. O. S. T., 2009: The SAMUM-1 experiment over Southern Morocco: Overview and
809 introduction. *Tellus*, **61B,** 2-11**,** doi:10.1111/j.1600-0889.2008.00403.x.

810 Hinds, W. C., 1999: *Aerosol Technology: Properties, Behaviour and Measurement of Airborne Particles.*
811 John Wiley & Sons, Inc., 483 pp.

812 Hoose, C., and O. Möhler, 2012: Heterogeneous ice nucleation on atmospheric aerosols: a review of
813 results from laboratory experiments. *Atmos. Chem. Phys.*, **12,** 9817-9854**,** doi:10.5194/acp-12-9817-
814 2012.

Huang, J. F., C. D. Zhang, and J. M. Prospero, 2010: African dust outbreaks: A satellite perspective of temporal and spatial variability over the tropical Atlantic Ocean. *J. Geophys. Res.*, **115,** D05202**,** doi:10.1029/2009jd012516.

Huneeus, N., M. Schulz, Y. Balkanski, J. Griesfeller, J. Prospero, S. Kinne, S. Bauer, O. Boucher, M. Chin, F. Dentener, T. Diehl, R. Easter, D. Fillmore, S. Ghan, P. Ginoux, A. Grini, L. Horowitz, D. Koch, M. C. Krol, W. Landing, and Coauthors, 2011: Global dust model intercomparison in AeroCom phase I. *Atmos. Chem. Phys.*, **11,** 7781-7816**,** doi:10.5194/acp-11-7781-2011.

IPCC, 2013: *Climate Change 2013: The Physical Science Basis. Contribution of Working Group I to the Fifth Assessment Report of the Intergovernmental Panel on Climate Change* Cambridge University Press.

Jähn, M., D. Muñoz-Esparza, F. Chouza, O. Reitebuch, O. Knoth, M. Haarig, and A. Ansmann, 2016: Investigations of boundary layer structure, cloud characteristics and vertical mixing of aerosols at Barbados with large eddy simulations. *Atmos. Chem. Phys.*, **16,** 651-674**,** doi:10.5194/acp-16-651-2016.

Jickells, T. D., Z. S. An, K. K. Andersen, A. R. Baker, G. Bergametti, N. Brooks, J. J. Cao, P. W. Boyd, R. A. Duce, K. A. Hunter, H. Kawahata, N. Kubilay, J. laRoche, P. S. Liss, N. Mahowald, J. M. Prospero, A. J. Ridgwell, I. Tegen, and R. Torres, 2005: Global Iron Connections Between Desert Dust, Ocean Biogeochemistry, and Climate. *Science*, **308,** 67-71**,** doi:10.1126/science.1105959.

Jung, E., B. Albrecht, J. M. Prospero, H. H. Jonsson, and S. M. Kreidenweis, 2013: Vertical structure of aerosols, temperature, and moisture associated with an intense African dust event observed over the eastern Caribbean. *J. Geophys. Res.*, **118,** 4623-4643**,** doi:10.1002/jgrd.50352.

Kaaden, N., A. Massling, A. Schladitz, T. Müller, K. Kandler, L. Schütz, B. Weinzierl, A. Petzold, M. Tesche, S. Leinert, C. Deutscher, M. Ebert, S. Weinbruch, and A. Wiedensohler, 2009: State of mixing, shape factor, number size distribution, and hygroscopic growth of the Saharan anthropogenic and mineral dust aerosol at Tinfou, Morocco. *Tellus*, **61B,** 51-63**,** doi:10.1111/j.1600-0889.2008.00388.x.

Kandler, K., K. Lieke, N. Benker, C. Emmel, M. Küpper, D. Müller-Ebert, M. Ebert, D. Scheuvens, A. Schladitz, L. Schütz, and S. Weinbruch, 2011: Electron microscopy of particles collected at Praia, Cape Verde, during the Saharan Mineral dust experiment: particle chemistry, shape, mixing state and complex refractive index. *Tellus*, **63B,** 475-496**,** doi:10.1111/j.1600-0889.2011.00550.x

Kandler, K., L. Schütz, C. Deutscher, M. Ebert, H. Hofmann, S. Jäckel, R. Jaenicke, P. Knippertz, K. Lieke, A. Massling, A. Petzold, A. Schladitz, B. Weinzierl, A. Wiedensohler, S. Zorn, and S. Weinbruch, 2009: Size distribution, mass concentration, chemical and mineralogical composition and derived optical parameters of the boundary layer aerosol at Tinfou, Morocco, during SAMUM 2006. *Tellus*, **61B,** 32-50**,** doi:10.1111/j.1600-0889.2008.00385.x.

Kanitz, T., R. Engelmann, B. Heinold, H. Baars, A. Skupin, and A. Ansmann, 2014: Tracking the Saharan Air Layer with shipborne lidar across the tropical Atlantic. *Geophys. Res. Lett.*, **41,** 1044-1050**,** doi:10.1002/2013gl058780.

852 Karyampudi, V. M., and T. N. Carlson, 1988: Analysis and Numerical Simulations of the Saharan Air
853 Layer and Its Effect on Easterly Wave Disturbances. *J. Atmos. Sci.*, **45,** 3102-3136.

854 Khan, B., G. Stenchikov, B. Weinzierl, S. Kalenderski, and S. Osipov, 2015: Dust plume formation in the
855 free troposphere and aerosol size distribution during the Saharan Mineral Dust Experiment in North
856 Africa. *Tellus*, **67B,** 27170**,** doi:10.3402/tellusb.v67.27170.

857 Kiladis, G. N., C. D. Thorncroft, and N. M. J. Hall, 2006: Three-Dimensional Structure and Dynamics of
858 African Easterly Waves. Part I: Observations. *J. Atmos. Sci.*, **63,** 2212-2230**,** doi:10.1175/JAS3741.1.

859 Knippertz, P., and M. C. Todd, 2010: The central west Saharan dust hot spot and its relation to African
860 easterly waves and extratropical disturbances. *J. Geophys. Res.*, **115,** D12117**,**
861 doi:10.1029/2009JD012819.

862 Kristensen, T. B., T. Müller, K. Kandler, N. Benker, M. Hartmann, J. M. Prospero, A. Wiedensohler, and
863 F. Stratmann, 2016: Properties of cloud condensation nuclei (CCN) in the trade wind marine boundary
864 layer of the western North Atlantic. *Atmos. Chem. Phys.*, **16,** 2675-2688**,** doi:10.5194/acp-16-2675-
865 2016.

866 Kumar, P., I. N. Sokolik, and A. Nenes, 2011: Measurements of cloud condensation nuclei activity and
867 droplet activation kinetics of fresh unprocessed regional dust samples and minerals. *Atmos. Chem.*
868 *Phys.*, **11,** 3527-3541**,** doi:10.5194/acp-11-3527-2011.

869 Levin, Z., E. Ganor, and V. Gladstein, 1996: The effects of desert particles coated with sulfate on rain
870 formation in the eastern Mediterranean. *J. Appl. Met.*, **35,** 1511-1523**,** doi:10.1175/1520-
871 0450(1996)035<1511:teodpc>2.0.co;2.

872 Lieke, K., K. Kandler, D. Scheuvens, C. Emmel, C. von Glahn, A. Petzold, B. Weinzierl, A. Veira, M. Ebert,
873 S. Weinbruch, and L. Schütz, 2011: Particle chemical properties in the vertical column based on aircraft
874 observations in the vicinity of Cape Verde Islands *Tellus*, **63B,** 497-511**,** doi:10.1111/j.1600-
875 0889.2011.00553.x.

876 Liu, Z., A. Omar, M. Vaughan, J. Hair, C. Kittaka, Y. Hu, K. Powell, C. Trepte, D. Winker, C. Hostetler, R.
877 Ferrare, and R. Pierce, 2008: CALIPSO lidar observations of the optical properties of Saharan dust: A
878 case study of long-range transport. *J. Geophys. Res.*, **113,** D07207**,** doi:10.1029/2007jd008878.

879 Maher, B. A., J. M. Prospero, D. Mackie, D. Gaiero, P. P. Hesse, and Y. Balkanski, 2010: Global
880 connections between aeolian dust, climate and ocean biogeochemistry at the present day and at the
881 last glacial maximum. *Earth-Sci. Rev.*, **99,** 61-97**,** doi:10.1016/j.earscirev.2009.12.001.

882 Mahowald, N., S. Albani, J. F. Kok, S. Engelstaeder, R. Scanza, D. S. Ward, and M. G. Flanner, 2014: The
883 size distribution of desert dust aerosols and its impact on the Earth system. *Aeolian Res.*, **15,** 53-71**,**
884 doi:10.1016/j.aeolia.2013.09.002.

885 Mamouri, R. E., and A. Ansmann, 2015: Estimated desert-dust ice nuclei profiles from polarization lidar:
886 methodology and case studies. *Atmos. Chem. Phys.*, **15,** 3463-3477**,** doi:10.5194/acp-15-3463-2015.

887 Maring, H., D. L. Savoie, M. A. Izaguirre, L. Custals, and J. S. Reid, 2003: Mineral dust aerosol size
888 distribution change during atmospheric transport. *J. Geophys. Res.*, **108,** 8592**,**
889 doi:10.1029/2002JD002536.

890 McConnell, C. L., E. J. Highwood, H. Coe, P. Formenti, B. Anderson, S. Osborne, S. Nava, K. Desboeufs,
891 G. Chen, and M. A. J. Harrison, 2008: Seasonal variations of the physical and optical characteristics of
892 Saharan dust: Results from the Dust Outflow and Deposition to the Ocean (DODO) experiment. *J.*
893 *Geophys. Res.*, **113,** D14505**,** doi:10.1029/2007jd009606.

894 Morman, S. A., and G. S. Plumlee, 2014: Dust and Human Health. *Mineral Dust: A Key Player in the*
895 *Earth System*, P. Knippertz, and W. J.-B. Stuut, Eds., Springer Netherlands, 385-409.

896 Müller, D., A. Ansmann, V. Freudenthaler, K. Kandler, C. Toledano, A. Hiebsch, J. Gasteiger, M.
897 Esselborn, M. Tesche, B. Heese, D. Althausen, B. Weinzierl, A. Petzold, and W. von Hoyningen-Huene,
898 2010: Mineral dust observed with AERONET Sun photometer, Raman lidar, and in situ instruments
899 during SAMUM 2006: Shape-dependent particle properties. *J. Geophys. Res.*, **115,** D11207**,**
900 doi:10.1029/2009jd012523.

901 Müller, T., A. Schladitz, N. Kaaden, and A. Wiedensohler, 2009: Spectral absorption coefficients and
902 imaginary parts of refractive indices of Saharan dust during SAMUM-1. *Tellus*, **61B,** 79-95**,**
903 doi:10.1111/j.1600-0889.2008.00399.x.

904 Myhre, G., D. Shindell, F.-M. Bréon, W. Collins, J. Fuglestvedt, J. Huang, D. Koch, J.-F. Lamarque, D. Lee,
905 B. Mendoza, T. Nakajima, A. Robock, G. Stephens, T. Takemura, and H. Zhang, 2013: *Anthropogenic*
906 *and Natural Radiative Forcing.* Cambridge University Press.

907 Nickovic, S., A. Vukovic, M. Vujadinovic, V. Djurdjevic, and G. Pejanovic, 2012: Technical Note: High-
908 resolution mineralogical database of dust-productive soils for atmospheric dust modeling. *Atmos.*
909 *Chem. Phys.*, **12,** 845-855**,** doi:10.5194/acp-12-845-2012.

910 Niedermeier, N., A. Held, T. Müller, B. Heinold, K. Schepanski, I. Tegen, K. Kandler, M. Ebert, S.
911 Weinbruch, K. Read, J. Lee, K. W. Fomba, K. Müller, H. Herrmann, and A. Wiedensohler, 2014: Mass
912 deposition fluxes of Saharan mineral dust to the tropical northeast Atlantic Ocean: an intercomparison
913 of methods. *Atmos. Chem. Phys.*, **14,** 2245-2266**,** doi:10.5194/acp-14-2245-2014.

914 Nousiainen, T., and K. Kandler, 2015: Light scattering by atmospheric mineral dust particles. *Light*
915 *Scattering Reviews 9: Light Scattering and Radiative Transfer*, A. A. Kokhanovsky, Ed., Springer Berlin
916 Heidelberg, 3-52.

917 Otto, S., M. de Reus, T. Trautmann, A. Thomase, M. Wendisch, and S. Borrmann, 2007: Atmospheric
918 radiative effects of an in-situ measured Saharan dust plume and the role of large particles. *Atmos.*
919 *Chem. Phys.*, **7,** 4887-4903**,** doi:10.5194/acp-7-4887-2007.

920 Peng, M. S., B. Fu, T. Li, and D. E. Stevens, 2012: Developing versus Nondeveloping Disturbances for
921 Tropical Cyclone Formation. Part I: North Atlantic. *Mon. Weather Rev.*, **140,** 1047-1066**,**
922 doi:10.1175/2011MWR3617.1.

Perry, K. D., S. S. Cliff, and M. P. Jimenez-Cruz, 2004: Evidence for hygroscopic mineral dust particles from the Intercontinental Transport and Chemical Transformation Experiment. *J. Geophys. Res.*, **109,** D23S28**,** doi:10.1029/2004jd004979.

Pöschl, U., 2005: Atmospheric Aerosols: Composition, Transformation, Climate and Health Effects. *Angew. Chem. Int. Ed.*, **44,** 7520-7540**,** doi:10.1002/anie.200501122.

Prospero, J. M., 1999: Long-range transport of mineral dust in the global atmosphere: Impact of African dust on the environment of the southeastern United States. *Proc. Natl. Acad. Sci. U. S. A.*, **96,** 3396-3403**,** doi:10.1073/pnas.96.7.3396.

Prospero, J. M., and T. N. Carlson, 1972: Vertical and areal distribution of Saharan dust over western equatorial North-Atlantic Ocean. *J. Geophys. Res.*, **77,** 5255-5265**,** doi:10.1029/JC077i027p05255.

Prospero, J. M., and P. J. Lamb, 2003: African droughts and dust transport to the Caribbean: Climate change implications. *Science*, **302,** 1024-1027**,** doi:10.1126/science.1089915.

Prospero, J. M., E. Bonatti, C. Schubert, and T. N. Carlson, 1970: Dust in the Caribbean atmosphere traced to an African dust storm. *Earth Planet. Sci. Lett.*, **9,** 287-293**,** doi:10.1016/0012-821X(70)90039-7.

Prospero, J. M., F. X. Collard, J. Molinie, and A. Jeannot, 2014: Characterizing the annual cycle of African dust transport to the Caribbean Basin and South America and its impact on the environment and air quality. *Glob. Biogeochem. Cycle*, **28,** 757-773**,** doi:10.1002/2013gb004802.

Raga, G. B., D. Baumgardner, and O. L. Mayol-Bracero, 2016: History of Aerosol-Cloud Interactions Derived from Observations in Mountaintop Clouds in Puerto Rico. *Aerosol Air Qual. Res.*, **16,** 674-688**,** doi:10.4209/aaqr.2015.05.0359.

Redelsperger, J.-L., C. D. Thorncroft, A. Diedhiou, T. Lebel, D. J. Parker, and J. Polcher, 2006: African Monsoon Multidisciplinary Analysis: An International Research Project and Field Campaign. *Bull. Am. Met. Soc.*, **87,** 1739-1746**,** doi:10.1175/BAMS-87-12-1739.

Reid, J. S., H. H. Jonsson, H. B. Maring, A. Smirnov, D. L. Savoie, S. S. Cliff, E. A. Reid, J. M. Livingston, M. M. Meier, O. Dubovik, and S. C. Tsay, 2003a: Comparison of size and morphological measurements of coarse mode dust particles from Africa. *J. Geophys. Res.*, **108,** 8593**,** doi:10.1029/2002JD002485.

Reid, J. S., J. E. Kinney, D. L. Westphal, B. Holben, E. J. Welton, S. Tsay, D. P. Eleuterio, J. R. Campbell, S. A. Christopher, P. R. Colarco, H. H. Jonsson, J. M. Livingston, H. B. Maring, M. L. Meier, P. Pilewskie, J. M. Prospero, E. A. Reid, L. A. Remer, G. Russell, D. Savoie, and Coauthors, 2003b: Analysis of measurements of Saharan dust by airborne and ground-based remote sensing methods during the Puerto Rico Dust Experiment (PRIDE). *J. Geophys. Res.*, **108,** 8586**,** doi:10.1029/2002JD002493.

Ryder, C. L., J. B. McQuaid, C. Flamant, P. D. Rosenberg, R. Washington, H. E. Brindley, E. J. Highwood, J. H. Marsham, D. J. Parker, M. C. Todd, J. R. Banks, J. K. Brooke, S. Engelstaedter, V. Estelles, P. Formenti, L. Garcia-Carreras, C. Kocha, F. Marenco, H. Sodemann, C. J. T. Allen, and Coauthors, 2015: Advances in understanding mineral dust and boundary layer processes over the Sahara from Fennec aircraft observations. *Atmos. Chem. Phys.*, **15,** 8479-8520**,** doi:10.5194/acp-15-8479-2015.

960 Sassen, K., P. J. DeMott, J. M. Prospero, and M. R. Poellot, 2003: Saharan dust storms and indirect
961 aerosol effects on clouds: CRYSTAL-FACE results. *Geophys. Res. Lett.*, **30,** 35-31**,**
962 doi:10.1029/2003gl017371.

963 Schepanski, K., I. Tegen, and A. Macke, 2012: Comparison of satellite based observations of Saharan
964 dust source areas. *Remote Sens. Environ.*, **123,** 90-97**,** doi:10.1016/j.rse.2012.03.019.

965 Schepanski, K., I. Tegen, B. Laurent, B. Heinold, and A. Macke, 2007: A new Saharan dust source
966 activation frequency map derived from MSG-SEVIRI IR-channels. *Geophys. Res. Lett.*, **34,** 1-5**,**
967 doi:10.1029/2007GL030168.

968 Schepanski, K., I. Tegen, M. C. Todd, B. Heinold, G. Bonisch, B. Laurent, and A. Macke, 2009:
969 Meteorological processes forcing Saharan dust emission inferred from MSG-SEVIRI observations of
970 subdaily dust source activation and numerical models. *J. Geophys. Res.*, **114,** D10201**,**
971 doi:10.1029/2008jd010325.

972 Scheuvens, D., L. Schütz, K. Kandler, M. Ebert, and S. Weinbruch, 2013: Bulk composition of northern
973 African dust and its source sediments — A compilation. *Earth-Sci. Rev.*, **116,** 170-194**,**
974 doi:10.1016/j.earscirev.2012.08.005.

975 Schladitz, A., T. Müller, A. Massling, N. Kaaden, K. Kandler, and A. Wiedensohler, 2009: In situ
976 measurements of optical properties at Tinfou (Morocco) during the Saharan Mineral Dust Experiment
977 SAMUM 2006. *Tellus*, **61B,** 64-78**,** doi:10.1111/j.1600-0889.2008.00397.x.

978 Schütz, L., 1980: Long-range transport of desert dust with special emphasis on the Sahara. *Ann. N.Y.*
979 *Acad. Sci.*, **338,** 515-532**,** doi:10.1111/j.1749-6632.1980.tb17144.x.

980 Seneviratne, S., N. Nicholls, D. Easterling, C. Goodess, S. Kanae, J. Kossin, Y. Luo, J. Marengo, K.
981 McInnes, and M. Rahimi, 2012: *Changes in climate extremes and their impacts on the natural physical*
982 *environment.* Managing the Risks of Extreme Events and Disasters to Advance Climate Change
983 Adaptation: A Special Report of Working Groups I and II of the Intergovernmental Panel on Climate
984 Change (IPCC), 109-230 pp.

985 Siebert, H., M. Beals, J. Bethke, E. Bierwirth, T. Conrath, K. Dieckmann, F. Ditas, A. Ehrlich, D. Farrell, S.
986 Hartmann, M. A. Izaguirre, J. Katzwinkel, L. Nuijens, G. Roberts, M. Schäfer, R. A. Shaw, T. Schmeissner,
987 I. Serikov, B. Stevens, F. Stratmann, and Coauthors, 2013: The fine-scale structure of the trade wind
988 cumuli over Barbados - an introduction to the CARRIBA project. *Atmos. Chem. Phys.*, **13,** 10061-10077**,**
989 doi:10.5194/acp-13-10061-2013.

990 Smirnov, A., B. N. Holben, D. Savoie, J. M. Prospero, Y. J. Kaufman, D. Tanre, T. F. Eck, and I. Slutsker,
991 2000: Relationship between column aerosol optical thickness and in situ ground based dust
992 concentrations over Barbados. *Geophys. Res. Lett.*, **27,** 1643-1646**,** doi:10.1029/1999gl011336.

993 Sokolik, I. N., D. M. Winker, G. Bergametti, D. A. Gillette, G. Carmichael, Y. J. Kaufman, L. Gomes, L.
994 Schuetz, and J. E. Penner, 2001: Introduction to special section: Outstanding problems in quantifying
995 the radiative impacts of mineral dust. *J. Geophys. Res.*, **106,** 18015-18028**,** doi:10.1029/2000JD900498.

996 Spiegel, J. K., N. Buchmann, O. L. Mayol-Bracero, L. A. Cuadra-Rodriguez, C. J. Valle Díaz, K. A. Prather,
997 S. Mertes, and W. Eugster, 2014: Do Cloud Properties in a Puerto Rican Tropical Montane Cloud Forest
998 Depend on Occurrence of Long-Range Transported African Dust? *Pure and Applied Geophysics*, **171,**
999 2443-2459**,** doi:10.1007/s00024-014-0830-y.

1000 Stevens, B., and G. Feingold, 2009: Untangling aerosol effects on clouds and precipitation in a buffered
1001 system. *Nature*, **461,** 607-613**,** doi:10.1038/nature08281.

1002 Stevens, B., D. Farrell, L. Hirsch, F. Jansen, L. Nuijens, I. Serikov, B. Brügmann, M. Forde, H. Linne, K.
1003 Lonitz, and J. M. Prospero, 2015: The Barbados Cloud Observatory -- Anchoring Investigations of Clouds
1004 and Circulation on the Edge of the ITCZ. *Bull. Am. Met. Soc.*, **97,** 787-801**,** doi:10.1175/BAMS-D-14-
1005 00247.1.

1006 Sullivan, R. C., M. J. K. Moore, M. D. Petters, S. M. Kreidenweis, G. C. Roberts, and K. A. Prather, 2009:
1007 Effect of chemical mixing state on the hygroscopicity and cloud nucleation properties of calcium
1008 mineral dust particles. *Atmos. Chem. Phys.*, **9,** 3303-3316**,** doi:10.5194/acp-9-3303-2009.

1009 Swap, R., M. Garstang, S. Greco, R. Talbot, and P. Kallberg, 1992: Saharan dust in the Amazon basin.
1010 *Tellus*, **44B,** 133-149**,** doi:10.1034/j.1600-0889.1992.t01-1-00005.x.

1011 Tanré, D., J. Haywood, J. Pelon, J. F. Léon, B. Chatenet, P. Formenti, P. Francis, P. Goloub, E. Highwood,
1012 and G. Myhre, 2003: Measurement and modeling of the Saharan dust radiative impact: Overview of
1013 the Saharan Dust Experiment (SHADE). *J. Geophys. Res.*, **108,** 8574**,** doi:10.1029/2002JD003273.

1014 Tegen, I., 2003: Modeling the mineral dust aerosol cycle in the climate system. *Quat. Sci. Rev.*, **22,**
1015 1821-1834**,** doi:10.1016/S0277-3791(03)00163-X.

1016 Tesche, M., A. Ansmann, D. Muller, D. Althausen, R. Engelmann, V. Freudenthaler, and S. Gross, 2009:
1017 Vertically resolved separation of dust and smoke over Cape Verde using multiwavelength Raman and
1018 polarization lidars during Saharan Mineral Dust Experiment 2008. *J. Geophys. Res.*, **114,** D13202**,**
1019 doi:10.1029/2009jd011862.

1020 Tesche, M., D. Müller, S. Gross, A. Ansmann, D. Althausen, V. Freudenthaler, B. Weinzierl, A. Veira, and
1021 A. Petzold, 2011: Optical and microphysical properties of smoke over Cape Verde inferred from
1022 multiwavelength lidar measurements. *Tellus*, **63B,** 677-694**,** doi:10.1111/j.1600-0889.2011.00549.x.

1023 Thorncroft, C. D., and M. Blackburn, 1999: Maintenance of the African easterly jet. *Q. J. R. Meteorol.*
1024 *Soc.*, **125,** 763-786**,** doi:10.1002/qj.49712555502.

1025 Toledano, C., M. Wiegner, S. Gross, V. Freudenthaler, J. Gasteiger, D. Müller, T. Müller, A. Schladitz, B.
1026 Weinzierl, B. Torres, and N. T. O'Neill, 2011: Optical properties of aerosol mixtures derived from sun-
1027 sky radiometry during SAMUM-2. *Tellus*, **63B,** 635-648**,** doi:10.1111/j.1600-0889.2011.00573.x.

1028 Twohy, C. H., S. M. Kreidenweis, T. Eidhammer, E. V. Browell, A. J. Heymsfield, A. R. Bansemer, B. E.
1029 Anderson, G. Chen, S. Ismail, P. J. DeMott, and S. C. Van Den Heever, 2009: Saharan dust particles
1030 nucleate droplets in eastern Atlantic clouds. *Geophys. Res. Lett.*, **36,** L01807**,**
1031 doi:10.1029/2008gl035846.

1032 Valle-Diaz, C. J., E. Torres-Delgado, S. M. Colon-Santos, T. Lee, J. L. Collett, W. H. McDowell, and O. L.
1033 Mayol-Bracero, 2016: Impact of Long-Range Transported African Dust on Cloud Water Chemistry at a
1034 Tropical Montane Cloud Forest in Northeastern Puerto Rico. *Aerosol Air Qual. Res.*, **16,** 653-664**,**
1035 doi:10.4209/aaqr.2015.05.0320.

1036 Walser, A., B. Weinzierl, D. Sauer, A. Spanu, and J. Gasteiger, 2016: A New Approach to Optical Particle
1037 Counter Parametrization and Calibration Evaluation. *Atmos. Meas. Tech.***,** in preparation.

1038 Wang, C., S. Dong, A. T. Evan, G. R. Foltz, and S.-K. Lee, 2012: Multidecadal Covariability of North
1039 Atlantic Sea Surface Temperature, African Dust, Sahel Rainfall, and Atlantic Hurricanes. *J. Climate*, **25,**
1040 5404-5415**,** doi:10.1175/JCLI-D-11-00413.1.

1041 Wang, W., A. T. Evan, C. Flamant, and C. Lavaysse, 2015: On the decadal scale correlation between
1042 African dust and Sahel rainfall: The role of Saharan heat low–forced winds. *Science Advances*, **1,**
1043 doi:10.1126/sciadv.1500646.

1044 Washington, R., C. Flamant, D. J. Parker, J. Marsham, J. B. McQuaid, H. Brindley, M. Todd, E. J.
1045 Highwood, C. L. Ryder, J.-P. Chaboreau, C. Kocha, M. Bechir, and A. Saci, 2012: Fennec - The Saharan
1046 Climate System. *CLIVAR Exchanges*, **60, 17,** 31-32.

1047 Weinzierl, B., A. Petzold, M. Esselborn, M. Wirth, K. Rasp, K. Kandler, L. Schütz, P. Koepke, and M.
1048 Fiebig, 2009: Airborne measurements of dust layer properties, particle size distribution and mixing
1049 state of Saharan dust during SAMUM 2006. *Tellus*, **61B,** 96-117**,** doi:10.1111/j.1600-
1050 0889.2008.00392.x.

1051 Weinzierl, B., D. Sauer, M. Esselborn, A. Petzold, A. Veira, M. Rose, S. Mund, M. Wirth, A. Ansmann, M.
1052 Tesche, S. Gross, and V. Freudenthaler, 2011: Microphysical and optical properties of dust and tropical
1053 biomass burning aerosol layers in the Cape Verde region – An overview of the airborne in-situ and lidar
1054 measurements during SAMUM-2. *Tellus*, **63B,** 589-618**,** doi:10.1111/j.1600-0889.2011.00566.x.

1055 Weinzierl, B., D. Sauer, A. Minikin, O. Reitebuch, F. Dahlkötter, B. Mayer, C. Emde, I. Tegen, J. Gasteiger,
1056 A. Petzold, A. Veira, U. Kueppers, and U. Schumann, 2012: On the visibility of airborne volcanic ash and
1057 mineral dust from the pilot's perspective in flight. *Phys. Chem. Earth*, **45–46,** 87-102**,**
1058 doi:10.1016/j.pce.2012.04.003.

1059 Wurzler, S., T. G. Reisin, and Z. Levin, 2000: Modification of mineral dust particles by cloud processing
1060 and subsequent effects on drop size distributions. *J. Geophys. Res.*, **105,** 4501-4512**,**
1061 doi:10.1029/1999jd900980.

1062 Yu, H. B., M. Chin, H. S. Bian, T. L. Yuan, J. M. Prospero, A. H. Omar, L. A. Remer, D. M. Winker, Y. K.
1063 Yang, Y. Zhang, and Z. B. Zhang, 2015: Quantification of trans-Atlantic dust transport from seven-year
1064 (2007-2013) record of CALIPSO lidar measurements. *Remote Sens. Environ.*, **159,** 232-249**,**
1065 doi:10.1016/j.rse.2014.12.010.

1066 Zipser, E. J., C. H. Twohy, S. C. Tsay, K. L. Thornhill, S. Tanelli, R. Ross, T. N. Krishnamurti, Q. Ji, G. Jenkins,
1067 S. Ismail, N. C. Hsu, R. Hood, G. M. Heymsfield, A. Heymsfield, J. Halverson, H. M. Goodman, R. Ferrare,
1068 J. P. Dunion, M. Douglas, R. Cifelli, and Coauthors, 2009: The Saharan Air Layer and the fate of African
1069 easterly waves. *Bull. Am. Met. Soc.*, **90,** 1137-1156**,** doi:10.1175/2009bams2728.1.

1070

1071

1072 **Tables**

1073 **Table 1. Overview of airborne mineral dust field experiments near the dust sources over**

1074 **Africa, the Atlantic Ocean, and in the Caribbean mainly focusing on the past two decades.**

| Campaign acronym | Time span | Region | Objective/Science focus | Overview |
|---|---|---|---|---|
| **Field experiments near the dust sources/Africa** | | | | |
| SAMUM-1 | May/Jun 2006 | Southern Morocco | Characterize Saharan aerosol near the source region and quantify dust-related radiative effects | Heintzenberg (2009) |
| AMMA-SOP0 | Jan/Feb 2006 | (South) West Africa | Characterize Saharan aerosol and biomass burning aerosols from West Africa | Redelsperger et al. (2006) |
| DABEX | Jan/Feb 2006 | Niger | same topic as AMMA-SOP0 | Haywood et al. (2008) |
| DODO | Feb and Aug 2006 | West Africa | Characterize Saharan dust in two seasons, constrain model simulations, quantify deposition of iron to the North Atlantic Ocean | McConnell et al. (2008) |
| GERBILS | Jun 2007 | North Africa | Geographic distribution and physical and optical properties of Saharan dust, impact on radiation, validation of satellite retrievals and numerical weather prediction models | Haywood et al. (2011) |
| FENNEC | Apr and Jun 2011, Jun 2012 | Algeria and Mauritania, | Improve understanding of the Saharan climate system through a synergy of observations and modelling | Washington et al. (2012); Ryder et al. (2015) |
| **Atlantic Ocean off the coast of Africa** | | | | |
| SHADE | Sep 2000 | Cabo Verde | Investigation of aerosol parameters relevant for the determination of the direct radiative effect | Tanré et al. (2003) |
| NAMMA | Aug-Sep 2006 | Cabo Verde | Improve understanding of the relationship between the African Easterly Waves, the SAL, and tropical cyclogenesis | Zipser et al. (2009) |
| SAMUM-2 | Jan/Feb 2008 | Cabo Verde | Characterize Saharan aerosol and biomass-burding aerosol over the Eastern Atlantic | Ansmann et al. (2011) |
| SAMUM-2b | May/Jun 2008 | Cabo Verde | Same as SAMUM-2, but summer measurements | Ansmann et al. (2011) |
| SALTRACE | Apr-Jul 2013, see Table 2 | Cabo Verde | Characterize dust properties before long-range transport with the same instrumentation as over the Caribbean | this study |
| ICE-D | Aug 2015 | Cabo Verde | Study influence of mineral dust on clouds and improve representation of dust-produced INP and CCN in models | Cotton (2016 ) |
| **Caribbean** | | | | |
| BOMEX | May – Jul 1969 | Barbados | Measure vertical distribution of Saharan dust in the Caribbean and quantify dust transport over Atlantic | Prospero and Carlson (1972) |
| PRIDE | Jun/Jul 2000 | Caribbean | Understand the issues of dust transport and radiative forcing in the north subtropical Atlantic Ocean | Reid et al. (2003b) |
| CRYSTAL-FACE | Jul 2002 | Southern Florida | Investigate ice nucleation potential of long-range transported Saharan dust | Sassen et al. (2003) |
| BACEX | Mar/Apr 2010 | Barbados | Observe cloud-aerosol interactions | Jung et al. (2013) |
| CARIBBA | Nov 2010/ Apr 2011 | Barbados | High resolution and collocated measurements of trade wind cumuli and aerosol to characterize aerosol-cloud interactions | Siebert et al. (2013) |
| SALTRACE | 2013-2014, see Table 2 | Barbados & Caribbean | Characterize properties of aged dust in the Caribbean, quantify the impact of “aging” on the radiation budget and cloud-microphysical processes, investigate the meteorological context of trans-Atlantic dust transport, and assess the roles of removal processes during transport | this study |

AMMA-SOP0: African Monsoon Multidisciplinary Analysis, Special observing period 0; BACEX: Barbados Aerosol Cloud Experiment; BOMEX: Barbados Oceanic and Meteorological Experiment; CARRIBA: Cloud, Aerosol, Radiation and tuRbulence in the trade wInd regime over Barbados; CRYSTAL-FACE: Cirrus Regional Study of Tropical Anvils and Cirrus Layers-Florida Area Cirrus Experiment; DABEX: Dust and Biomass-burning Experiment; DODO: Dust Outflow and Deposition to the Ocean; Fennec: not an acronym; GERBILS: Geostationary Earth Radiation Budget Intercomparison of Longwave and Shortwave radiation; ICE-D: Ice in Cloud Experiments – Dust; NAMMA: NASA AMMA; PRIDE: Puerto Rico Dust Experiment; SAMUM: Saharan Mineral Dust Experiment; SHADE: SaHAran Dust Experiment

1075

1076

1077 **Table 2. Airborne, ground-based, and ship-borne measurements in the context of SALTRACE**

| Activity | Time | Observations, location | Stratification |
|---|---|---|---|
| METEOR-cruise | 29 Apr – 23 May 2013 | Ship-borne lidar, Guadeloupe – Cabo Verde | Dust above marine |
| SALTRACE | 10 Jun – 15 Jul 2013 | SALTRACE column experiment (ground-based and airborne in-situ & remote sensing observations), for measurement locations see Figure 1 | Dust above marine |
| SALTRACE-2 | 15 Feb – 8 Mar 2014 | Ground-based lidar & sun photometers, Barbados | Smoke/dust above marine |
| SALTRACE-3 | 19 Jun – 12 Jul 2014 | Ground-based lidar & sun photometers, Barbados | Dust above marine |

1078

## List of figures

Figure 1. Flight tracks (red lines) of the airborne SALTRACE observations in summer 2013 with the ground-sites Barbados (main super-site), Cabo Verde and Puerto Rico indicated. Furthermore, the locations of the SAMUM measurements in Morocco (2006) and Cabo Verde (2008) are shown.

Figure 2. Map with SALTRACE measurement locations on Barbados. a) Photograph of trade-wind cumuli over Barbados which were frequently observed. b) Lidar and sun photometer container at Caribbean Institute for Hydrology and Meteorology Barbados (13°8‘55‘‘N, 59°37‘29‘‘W). The green line is the laser beam from the TROPOS lidar instrument. c) Measurement tower with the ground-based in-situ measurements at Ragged Point (13°09’54’’N, 59°25’56’’W). d) The DLR Falcon research aircraft taking off at Barbados (13°4’32’’N, 59°29'30''W) on 20 June 2013.

Figure 3. Summer (June-July-August) mean dust concentrations at Barbados from 1965 to 2013 with the years of the airborne field experiments SAMUM and SALTRACE indicated.

Figure 4. Aerosol optical depth (AOD, 500 nm) throughout SALTRACE at Cabo Verde, Barbados, and Puerto Rico together with a time-height cross-section of volume linear depolarization ratio (VLDR, 532 nm) illustrating the dust layer at Barbados. The red triangles in the three time series indicate the median AOD during the duration of the Falcon flights. For Barbados, also the dust mass concentration near the ground at Ragged Point is shown (blue circles). Lidar sequences in which clouds shielded the dust layer were removed. To better visualize the time evolution of the dust layer, the lidar data were linearly interpolated in periods without data. Interpolation was only performed if AOD time series suggested that no major changes were taking place. White-shaded areas mark interpolated sequences.

Figure 5. Regions of most active dust sources during SALTRACE (red contours), SAMUM-1 (green contours), and SAMUM-2 (blue contours). The gray-shaded areas indicate all source regions active during SALTRACE regardless their emission intensity and activation frequency. Solid contour lines represent the orography with altitudes (in m ASL) indicated.

Figure 6. Top: lidar cross-sections of dust layer structure in the Cabo Verde region (right) and Barbados (left) together with a photograph of dust layers in the Caribbean (mid) during SALTRACE in summer 2013. Bottom: schematics of dust “aging” processes during transport from Africa into the Caribbean.

Figure 7. Time-altitude cross sections of volume linear depolarization ratio (VLDR) detected with the TROPOS lidar BERTHA at three different locations between Africa and the Caribbean (Ouarzazate/Morocco, Praia/Cabo Verde, Barbados) in summer 2006, 2008, 2013 and 2014 and in winter 2008 and 2014. The aerosol extends from the ground to 3-5 km altitude. The top of the aerosol layers is indicated by the white dashed lines. Note: VLDR values in Morocco and Cabo Verde were measured at a wavelength of 710 nm, whereas the VLDR values in Barbados refer to 1064 nm.

Figure 8. COSMO-MUSCAT simulations showing the trans-Atlantic dust transport for the Lagrangian dust sampling flights between 17 and 22 June 2013. Color-coded dust AOD maps are combined with longitude-altitude cross-sections through the dust layer which show model dust mass concentrations.

Figure 9. Mineral dust size distribution detected with a combination of instruments before and after trans-Atlantic transport: the size distribution between 0.01 – 1 µm was determined from the data of a CPC, a Grimm Sky OPC and a UHSAS-A using a consistent Bayesian inversion procedure (Walser et al., 2016); for the coarse mode above 1 µm, data points and uncertainty ranges from the CAS-DPOL spectrometer are shown. The air mass studied in the Cabo Verde region (blue symbols) on 17 June 2013 was sampled again five days later above Barbados (red symbols). According to Stokes gravitational settling, no particles larger than 7 µm should be present at an altitude of about 1.3 km

below the SAL top, i.e. at the altitude where these measurements in Barbados were taken. Number concentrations are given for standard pressure and temperature conditions (1013 hPa, 273 K).

Figure 10. Composition / volatility size distribution for the Lagrangian observations. The samples were collected near Cabo Verde (left) at 2.6 km altitude and near Barbados (right) at 2.3 km altitude. Top: chemical particle groups are shown in color, volatility observations are given in black and white ('small inclusion' referring to less than 30% of the particle volume, 'large inclusion' to 30% - 90%, and 'coating' to more than 90% of the volume being refractory). Bottom: composition of the refractory residuals with particle sizes given as projected area diameter. The numbers above the diagram are the particle counts for each bar; they cannot be considered as number size distribution.

Figure 11. Top: Measurements of volume linear depolarization ratio (VLDR) and attenuated backscatter coefficient detected with the LMU lidar POLIS before, during and after the passage of tropical storm Chantal, and on 11 July 2013 during the time of the first Falcon flight (Figure 12). Bottom: Meteosat SAL-tracking satellite image (courtesy of the University of Wisconsin – CIMSS) overlaid with contours of modelled dust AOD (500 nm, green contours) from the regional Saharan dust model COSMO-MUSCAT. The Falcon flight track is indicated in turquoise.

Figure 12. Vertical profiles of extinction coefficient and PLDR detected with the POLIS lidar, aerosol number concentration detected with several instruments in different size classes, and CCN number concentration at 0.2% supersaturation (SS) for high (red) and low (blue) dust loads taken over Barbados on 8 and 11 July 2013 (see also Figure 11 for the periods of the Falcon flights on those days). The corresponding ground-based measurements at Ragged Point are shown with green symbols. Date collected during sequences at constant altitude were averaged and are indicated with big symbols. The error bars indicate the 16- and 84-percentile values within the individual horizontal level. The grey-shaded areas sketch the overlap of the lidar and the range where the Constant Pressure Inlet (CPI) of the CCN counter did no longer keep the CCNC at a constant pressure of 500 hPa. All data are given for ambient conditions.

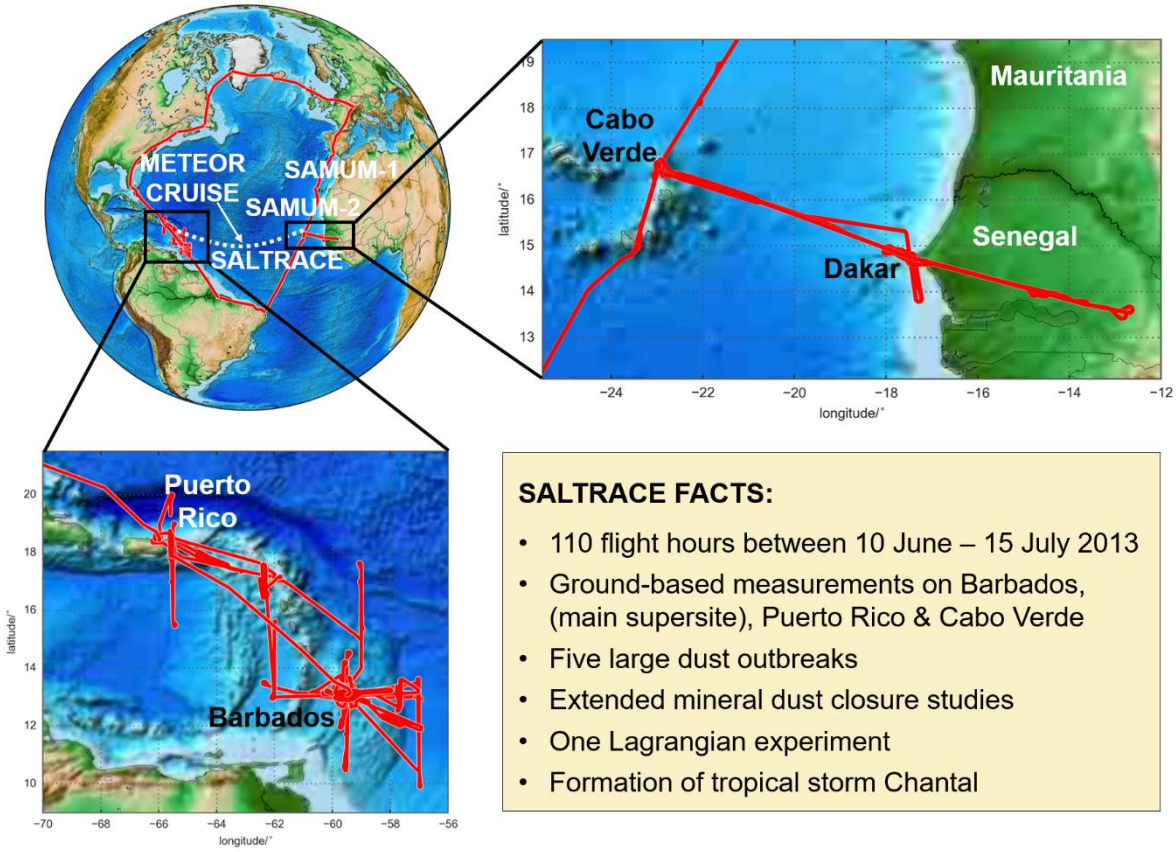


**Figure 1. Flight tracks (red lines) of the airborne SALTRACE observations[2] in summer 2013 with the ground-sites Barbados (main super-site), Cabo Verde and Puerto Rico indicated. Furthermore, the locations of the SAMUM measurements in Morocco (2006) and Cabo Verde (2008) are shown.**

[2] Note: no data are available in Brazilian airspace.

1157

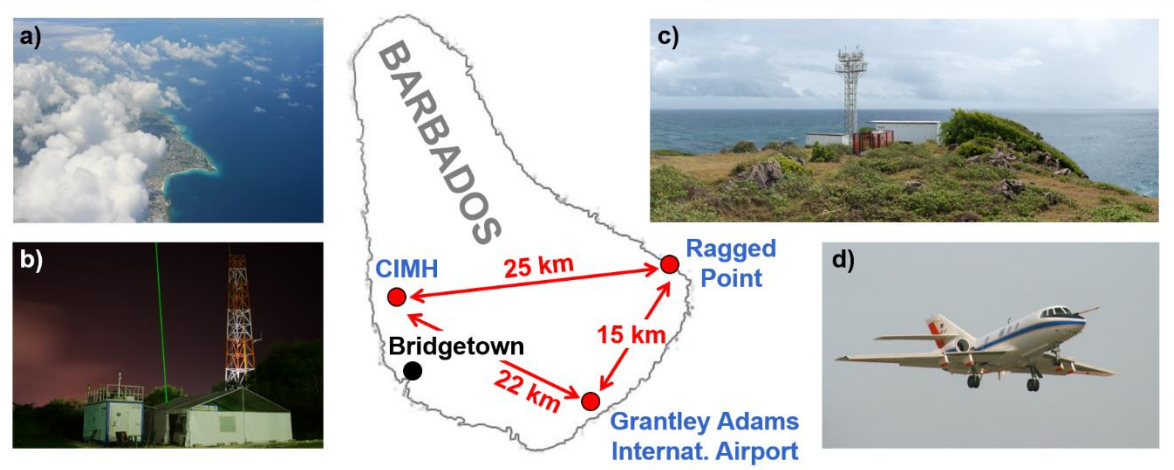


1158

1159 **Figure 2. Map with SALTRACE measurement locations on Barbados. a) Photograph of trade-**
1160 **wind cumuli over Barbados which were frequently observed. b) Lidar and sun photometer**
1161 **container at Caribbean Institute for Hydrology and Meteorology Barbados (13°8‘55‘‘N,**
1162 **59°37‘29‘‘W). The green line is the laser beam from the TROPOS lidar instrument. c)**
1163 **Measurement tower with the ground-based in-situ measurements at Ragged Point**
1164 **(13°09’54’’N, 59°25’56’’W). d) The DLR Falcon research aircraft taking off at Barbados**
1165 **(13°4’32’’N, 59°29'30''W) on 20 June 2013.**

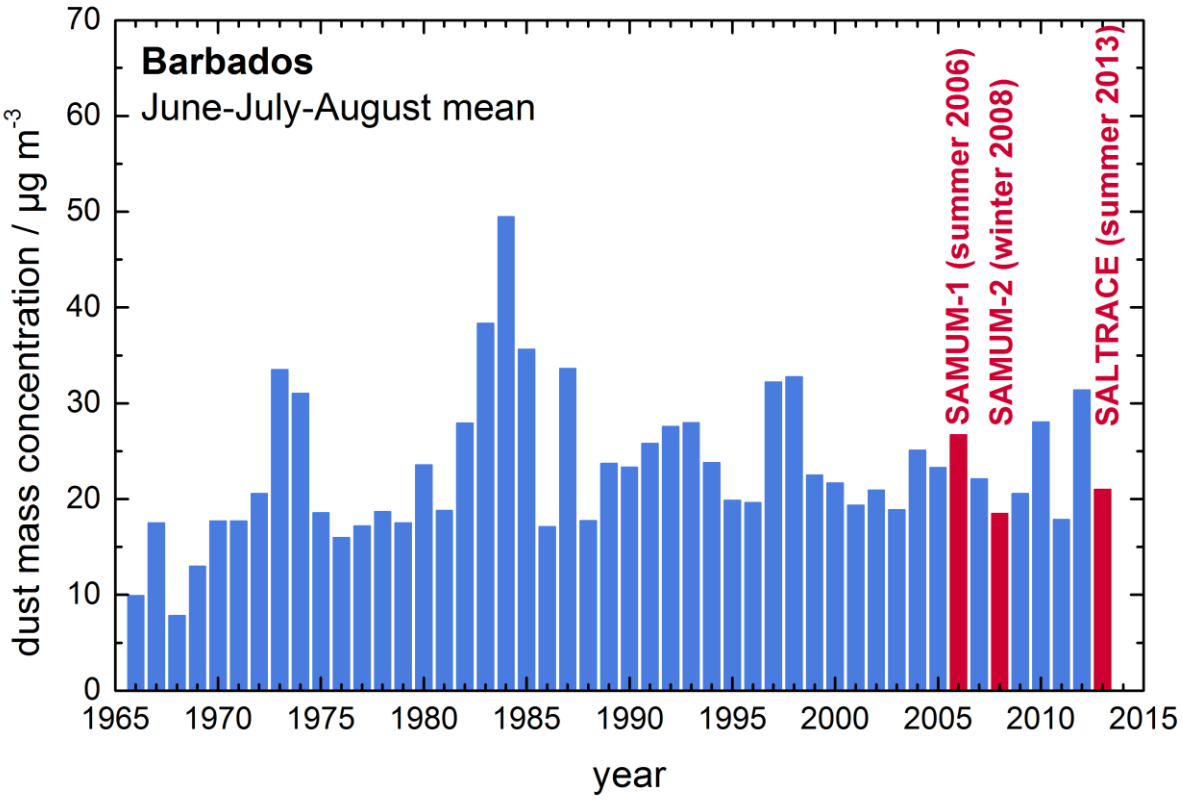


**Figure 3. Summer (June-July-August) mean dust concentrations at Barbados from 1965 to 2013 with the years of the airborne field experiments SAMUM and SALTRACE indicated.**

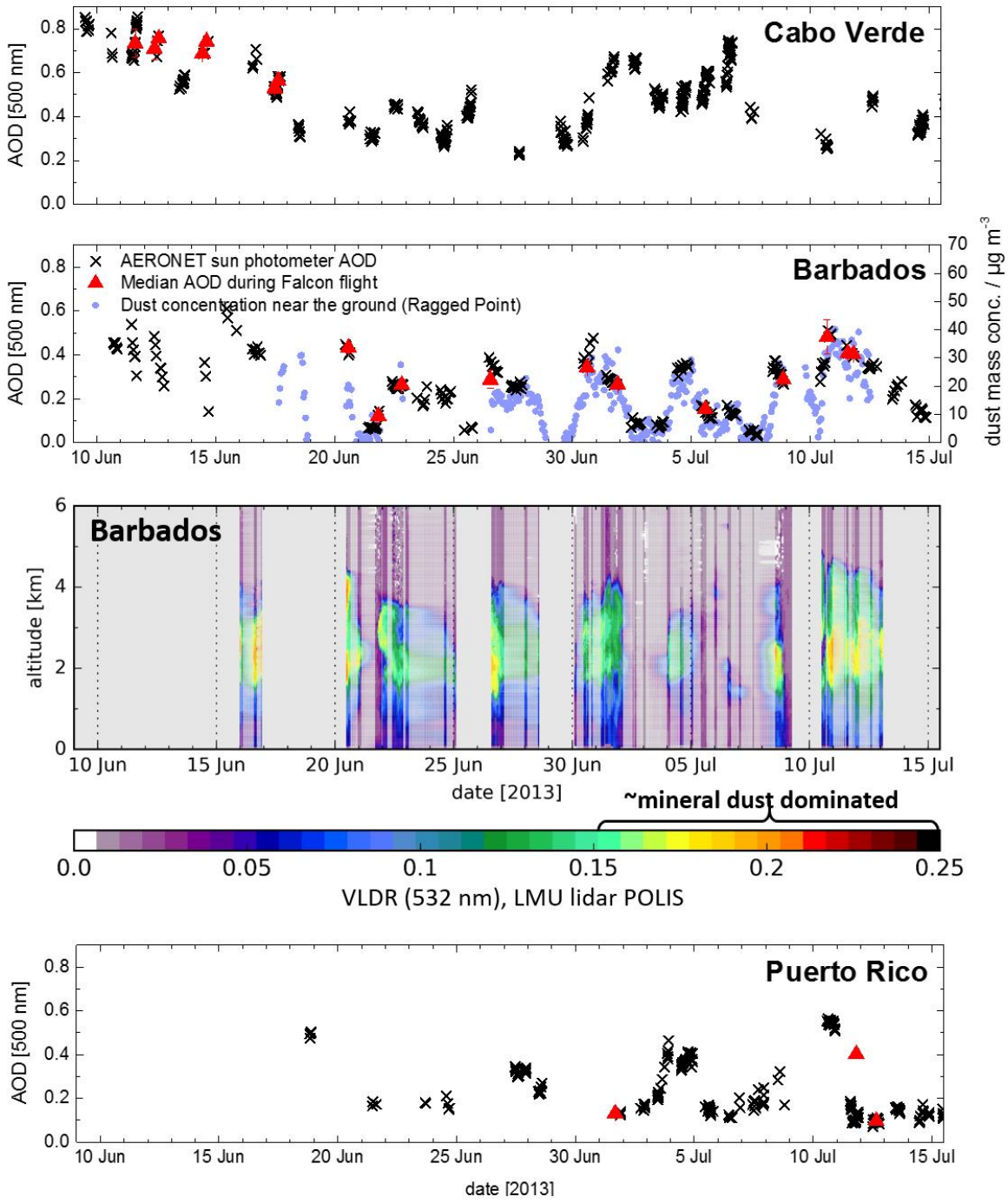


1169

1170 **Figure 4. Aerosol optical depth (AOD, 500 nm) throughout SALTRACE at Cabo Verde,**
1171 **Barbados, and Puerto Rico together with a time-height cross-section of volume linear**
1172 **depolarization ratio (VLDR, 532 nm) illustrating the dust layer at Barbados. The red triangles**
1173 **in the three time series indicate the median AOD during the duration of the Falcon flights.**
1174 **For Barbados, also the dust mass concentration near the ground at Ragged Point is shown**

**(blue circles). Lidar sequences in which clouds shielded the dust layer were removed. To better visualize the time evolution of the dust layer, the lidar data were linearly interpolated in periods without data. Interpolation was only performed if AOD time series suggested that no major changes were taking place. White-shaded areas mark interpolated sequences.**

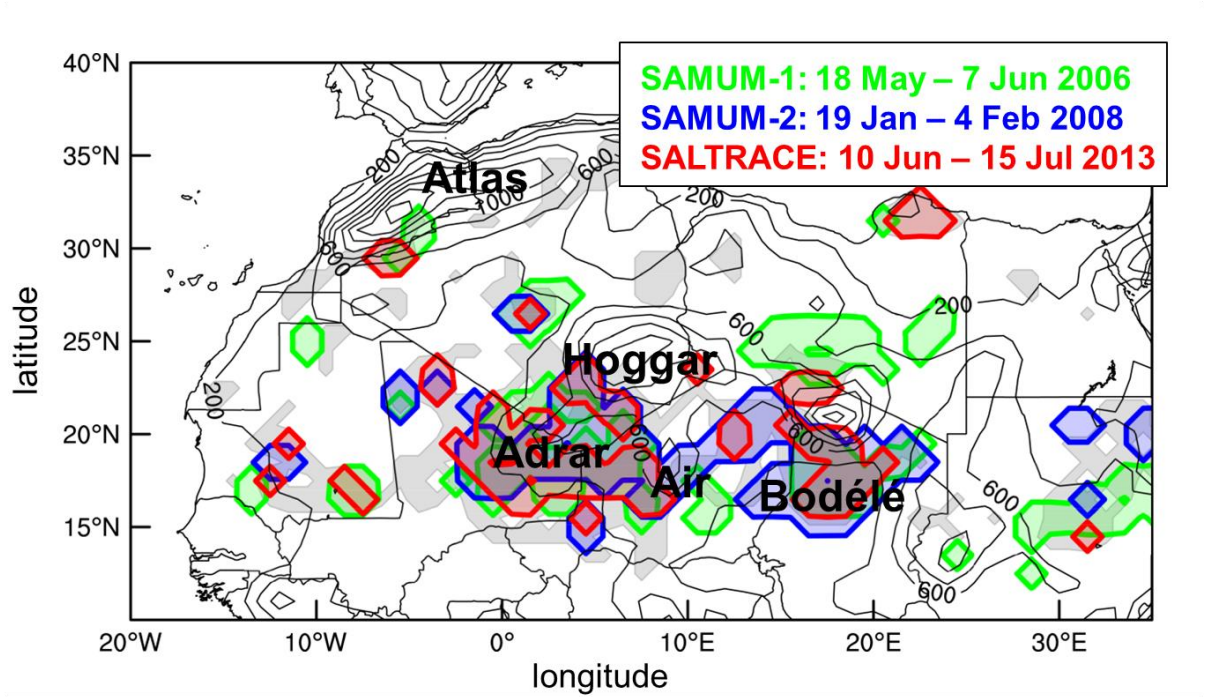


1188

1189 **Figure 5. Regions of most active dust sources during SALTRACE (red contours), SAMUM-1**
1190 **(green contours), and SAMUM-2 (blue contours). The gray-shaded areas indicate all source**
1191 **regions active during SALTRACE regardless their emission intensity and activation**
1192 **frequency. Solid contour lines represent the orography with altitudes (in m ASL) indicated.**

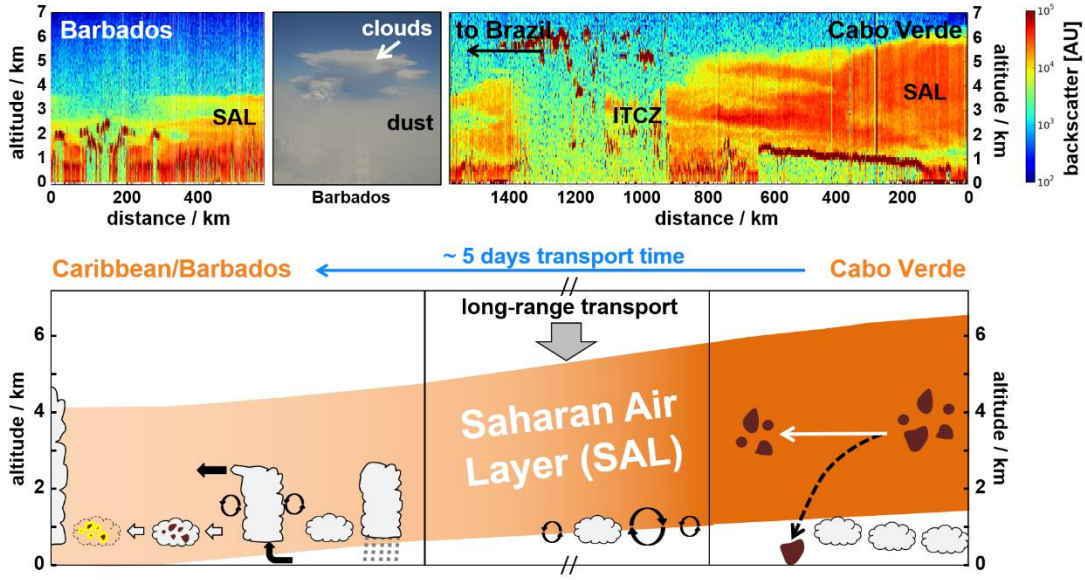


1193

1194 **Figure 6. Top: lidar cross-sections of dust layer structure in the Cabo Verde region (right)**

1195 **and Barbados (left) together with a photograph of dust layers in the Caribbean (mid)**

1196 **during SALTRACE in summer 2013. Bottom: schematics of dust "aging" processes during**

1197 **transport from Africa into the Caribbean.**

1198

1199

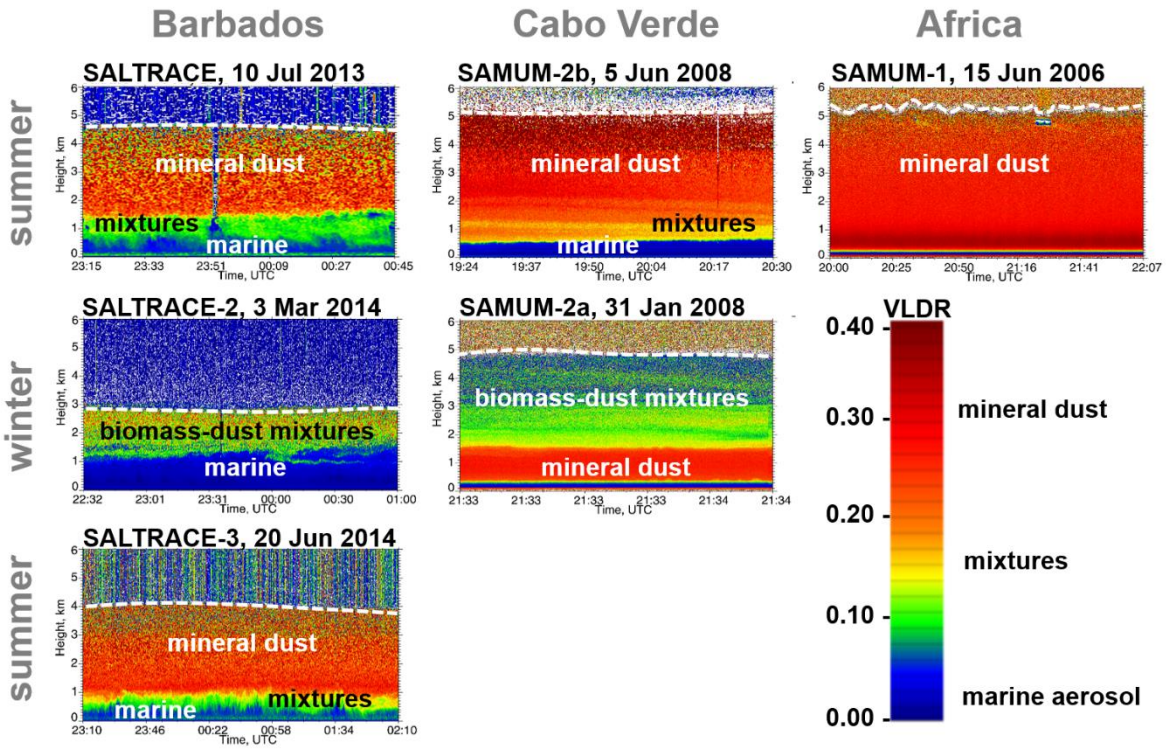


1200

1201 **Figure 7. Time-altitude cross sections of volume linear depolarization ratio (VLDR) detected**
1202 **with the TROPOS lidar BERTHA at three different locations between Africa and the**
1203 **Caribbean (Ouarzazate/Morocco, Praia/Cabo Verde, Barbados) in summer 2006, 2008, 2013**
1204 **and 2014 and in winter 2008 and 2014. The aerosol extends from the ground to 3-5 km**
1205 **altitude. The top of the aerosol layers is indicated by the white dashed lines. Note: VLDR**
1206 **values in Morocco and Cabo Verde were measured at a wavelength of 710 nm, whereas the**
1207 **VLDR values in Barbados refer to 1064 nm.**

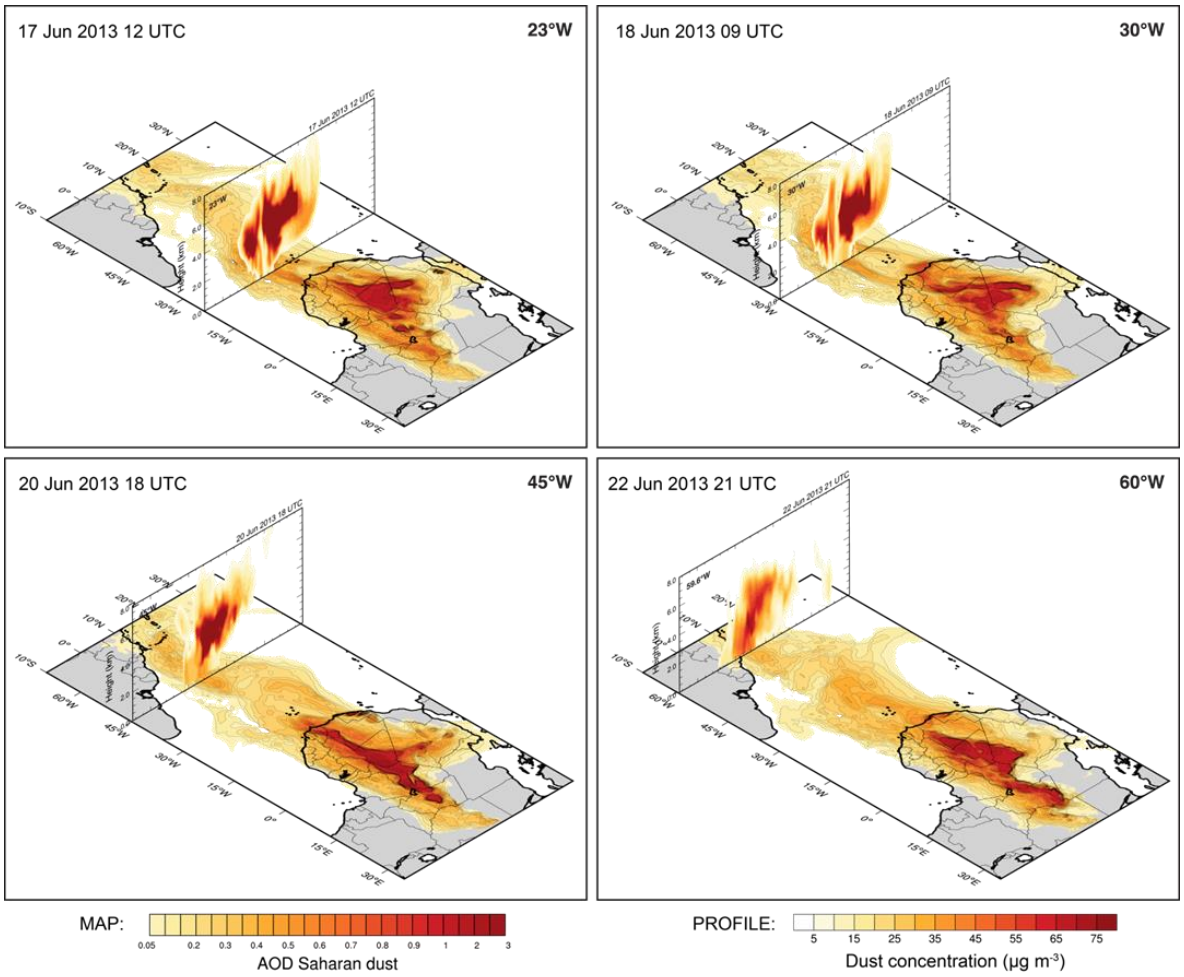


1208

1209 **Figure 8. COSMO-MUSCAT simulations showing the trans-Atlantic dust transport for the**
1210 **Lagrangian dust sampling flights between 17 and 22 June 2013. Color-coded dust AOD maps**
1211 **are combined with longitude-altitude cross-sections through the dust layer which show**
1212 **model dust mass concentrations.**

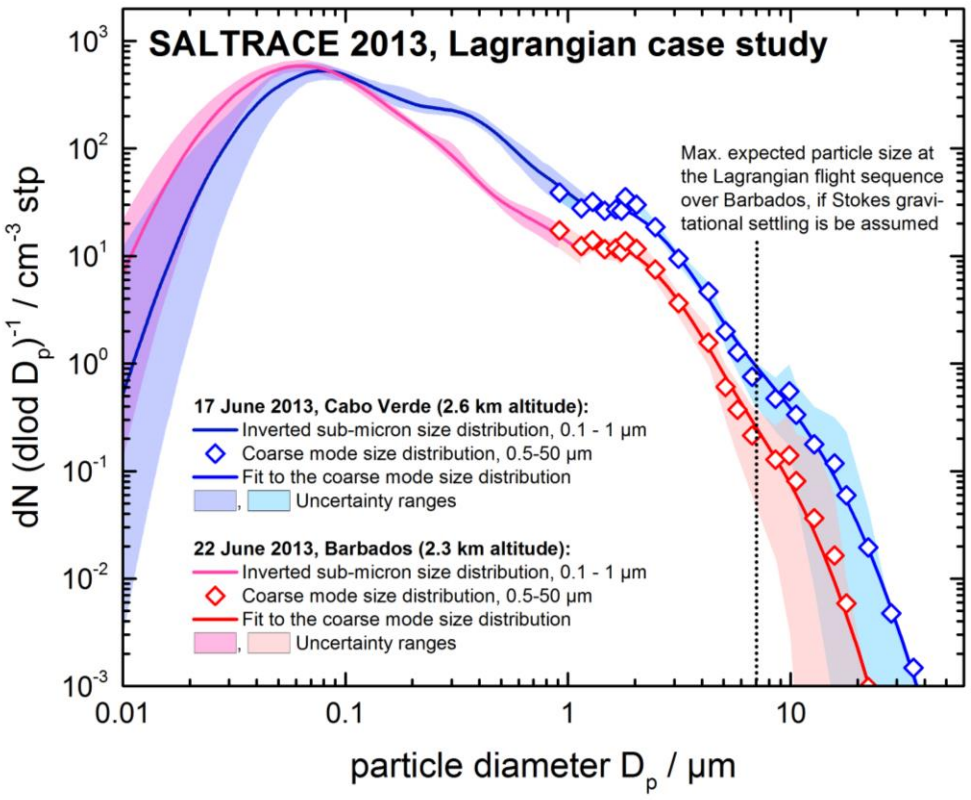


**Figure 9. Mineral dust size distribution detected with a combination of instruments before and after trans-Atlantic transport: the size distribution between 0.01 – 1 µm was determined from the data of a CPC, a Grimm Sky OPC and a UHSAS-A using a consistent Bayesian inversion procedure (Walser et al., 2016); for the coarse mode above 1 µm, data points, 10 and 90 percentile concentration values from the CAS-DPOL spectrometer, and a fits to the coarse mode size distribution data are shown. The air mass studied in the Cabo Verde region (blue symbols) on 17 June 2013 was sampled again five days later above Barbados (red symbols). According to Stokes gravitational settling, no particles larger than 7 µm should be present at an altitude of about 1.3 km below the SAL top, i.e. at the altitude where these measurements in Barbados were taken. Number concentrations are given for standard pressure and temperature conditions (1013 hPa, 273 K).**

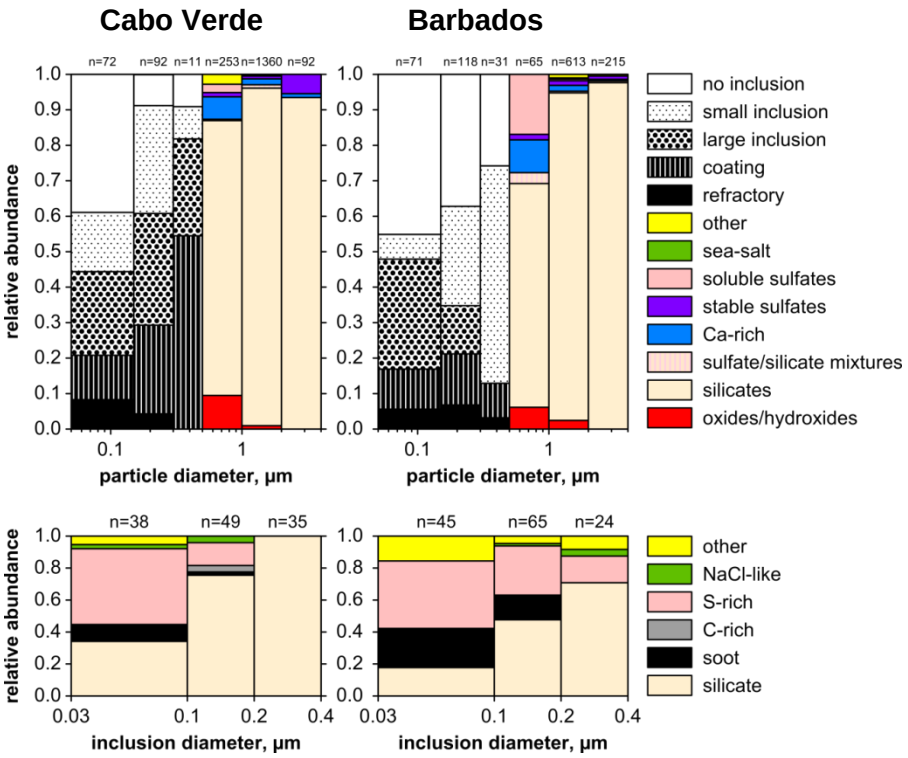


**Figure 10. Composition / volatility size distribution for the Lagrangian observations. The samples were collected near Cabo Verde (left) at 2.6 km altitude and near Barbados (right) at 2.3 km altitude. Top: chemical particle groups are shown in color, volatility observations are given in black and white ('small inclusion' referring to less than 30% of the particle volume, 'large inclusion' to 30% - 90%, and 'coating' to more than 90% of the volume being refractory). Bottom: composition of the refractory residuals with particle sizes given as projected area diameter. The numbers above the diagram are the particle counts for each bar; they cannot be considered as number size distribution.**

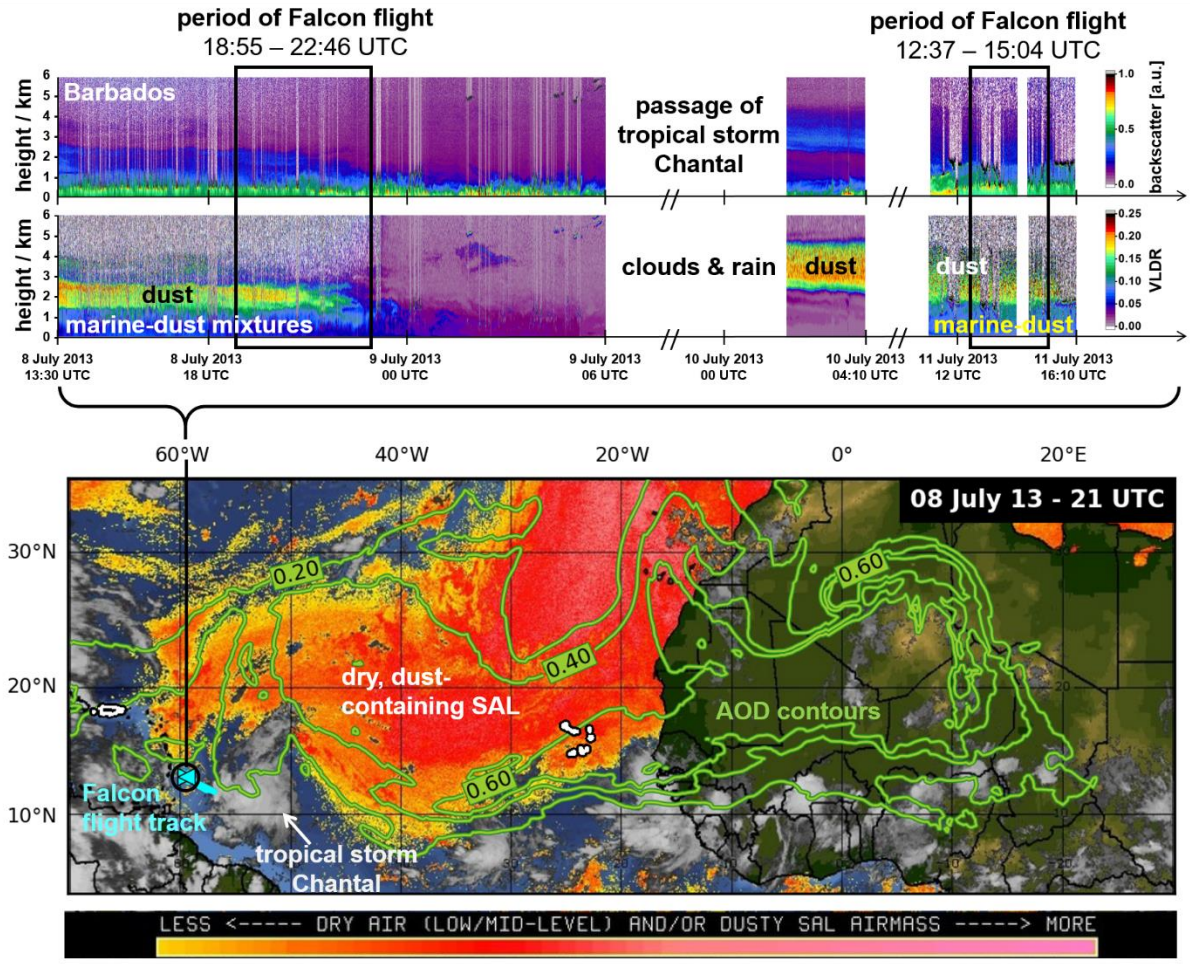


**Figure 11. Top: Measurements of volume linear depolarization ratio (VLDR) and attenuated backscatter coefficient detected with the LMU lidar POLIS before, during and after the passage of tropical storm Chantal, and on 11 July 2013 during the time of the first Falcon flight (Figure 12). Bottom: Meteosat SAL-tracking satellite image (courtesy of the University of Wisconsin – CIMSS) overlaid with contours of modelled dust AOD (500 nm, green contours) from the regional Saharan dust model COSMO-MUSCAT. The Falcon flight track is indicated in turquoise.**

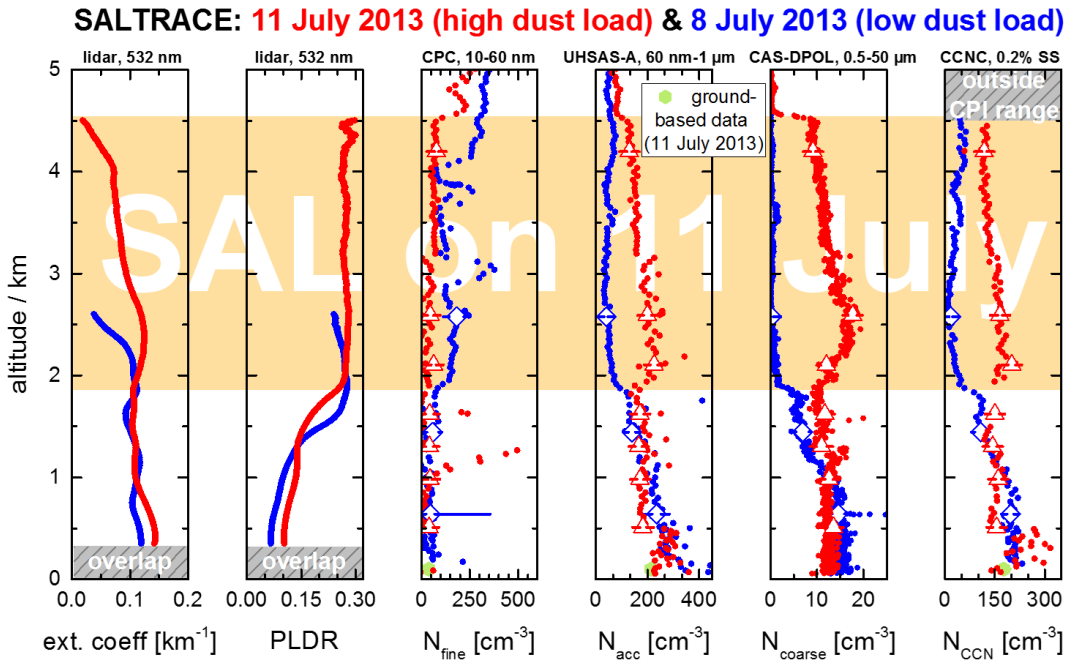


1244

1245 **Figure 12. Vertical profiles of extinction coefficient and PLDR detected with the POLIS lidar,**
1246 **aerosol number concentration detected with several instruments in different size classes,**
1247 **and CCN number concentration at 0.2% supersaturation (SS) for high (red) and low (blue)**
1248 **dust loads taken over Barbados on 8 and 11 July 2013 (see also Figure 11 for the periods of**
1249 **the Falcon flights on those days). The corresponding ground-based measurements at Ragged**
1250 **Point are shown with green symbols. Date collected during sequences at constant altitude**
1251 **were averaged and are indicated with big symbols. The error bars indicate the 16- and 84-**
1252 **percentile values within the individual horizontal level. The grey-shaded areas sketch the**
1253 **overlap of the lidar and the range where the Constant Pressure Inlet (CPI) of the CCN counter**
1254 **did no longer keep the CCNC at a constant pressure of 500 hPa. All data are given for ambient**
1255 **conditions.**